Final Report

Project Title

MODELING THE DISPERSION OF VAPOR AND AEROSOL PARTICULATES IN THE ATMOSPHERIC BOUNDARY LAYER

Grant number

N00014-98-1-0557

Submitted to

Dr. Scott Sandgathe

Program Director, Office of Naval Research

Principal Investigators

Steven Chai and Darko Koracin

Division of Atmospheric Sciences
Desert Research Institute
University and Community College Systems of Nevada
2215 Raggio Parkway
Reno, NV 89512-1095

Consultants

Leif Enger and Matthias Mohr
Department of Earth Sciences - Meteorology
Uppsala University
Uppsala, Sweden

REPORT DOCUMENTATION PAGE

Form Approved
OMB No. 0704-0188

1. AGENCY USE ONLY *(Leave Blank)*	2. REPORT DATE May 17, 2001	3. REPORT TYPE AND DATES COVERED Final Technicall: 05/01/98 - 04/30/01

4. TITLE AND SUBTITLE
Modeling the dispersion of vapor and aerosol particulates in the atmospheric boundary layer

5. FUNDING NUMBERS
G N00014-98-1-0557

6. AUTHORS
Steven K. Chai
Darko Koracin
Leif Enger

7. PERFORMING ORGANIZATION NAME(S) AND ADDRESS(ES)
Desert Research Institute
University and Community College System of Nevada
2215 Raggio Parkway
Reno, NV 89512-1095

8. PERFORMING ORGANIZATION REPORT NUMBER
N/A

9. SPONSORING / MONITORING AGENCY NAME(S) AND ADDRESS(ES)
Office of Naval Research
800 North Quincy Street
Arlington, VA 22217-5660

10. SPONSORING / MONITORING AGENCY REPORT NUMBER

11. SUPPLEMENTARY NOTES
None

12a. DISTRIBUTION / AVAILABILITY STATEMENT
Unlimited

12b. DISTRIBUTION CODE

13. ABSTRACT *(Maximum 200 words)*
Report attached.

14. SUBJECT TERMS
Dispersion Modeling; Boundary Layer; Complex Terrain

15. NUMBER OF PAGES
47

16. PRICE CODE

17. SECURITY CLASSIFICATION OF REPORT	18. SECURITY CLASSIFICATION OF THIS PAGE	19. SECURITY CLASSIFICATION OF ABSTRACT	20. LIMITATION OF ABSTRACT
Unclassified	Unclassified	Unclassified	

1. Project Summary

The goal of this project is to improve our scientific understanding of dispersion issues over complex terrain and publish results in scientific journals. Three scientific articles and one student's Master thesis are under preparation based on the results supported by this project.

The first paper, entitled "The role of advection of fluxes on modeling dispersion in convective boundary layers", is aimed at examining the importance of the advection terms for dispersion in a convective boundary layer. An Eulerian three-dimensional higher-order closure dispersion model is presented. The model uses mean wind and turbulence values from a second order atmospheric boundary layer model. The dispersion model is validated against results from tank and field experiments and compared to results from Lagrangian dispersion models. The results show good agreement with experiment and Lagrangian modeling results for point source dispersion in a convective boundary layer. Sensitivity studies of the model helped to identify the roles that advection and horizontal transport terms in the equations for the fluxes play in simulating the essential features of pollutant dispersion. The results from the sensitivity tests show that the famous features of dispersion from a point source in the convective boundary layer - with an ascending plume during ground level release and descending for a lifted point source - is caused by the advection term in the equation for the vertical flux. Furthermore, it is shown that there is a tendency for the plume to split horizontally, which is also caused by the advection term in horizontal fluxes.

The article entitled "Modeling of atmospheric pollutant dispersion in complex terrain – Development, validation and comparison of a higher-order closure mesoscale model" is a two part paper. In part I, data from the extensive field program MOHAVE (Measurements Of Haze And Visibility Experiment) was used to evaluate the meteorological output of two atmospheric mesoscale models, the higher-order MIUU model (Meteorological Institute of Uppsala University's model) and the MM5 (the fifth-generation Penn State/NCCAR Mesoscale Model). Part II presented a higher-order closure dispersion model suitable for modeling dispersion in complex terrain. The results of this model have been compared against tank experiment as well as the MOHAVE data.

In the student's Master thesis a trajectory model is developed. This model has two-dimensional (on an isentropic surface) and three-dimensional options. This model has many applications such as tracing the dust trajectory from the Gobi desert.

The content of the first paper will be presented in Section 2. The other two papers, which are still under preparation, will be reported in Section 3. The thesis will be reported in Section 4.

2. The role of advection of fluxes on modeling dispersion in convective boundary layers

2.1 Introduction

In recent years, due to an increased interest in environmental problems, considerable attention has been focussed on means of predicting concentration levels in turbulent boundary layers. In practice, predictions are often required for dispersion in complicated flows over coastal areas or other complex terrain, since air pollution sources are often situated in such areas. To obtain the flow fields over complex terrain one usually solves a complete set of hydrodynamic and thermodynamic equations. This provides the meteorological parameters needed for the dispersion calculations. The dispersion calculations follow different lines:

One type of approach is to use the standard Gaussian dispersion model, modified to account for terrain influences. Examples of such models are described by Egan (1984), Hunt et al. (1979), Mistra (1980), Andrén (1987), and Enger (1990c). With this approach, terrain adjustment factors are introduced to correct for the calculation of standard deviation of the Gaussian concentration distribution. The weakness of this approach is that the adjustment factors are site-dependent. Furthermore, most of these types of models are only applicable on the idealized topography on which they are formulated.

Another approach is to use Lagrangian particle dispersion models. Atmospheric dispersion in a Lagrangian model is simulated by tracing a large set of particles driven by wind and turbulence fields predicted by the atmospheric model. Subsequent positions of each particle, representing a discrete element of pollutant mass, are computed from the relations. The resolvable scale components of wind velocity are obtained directly from the mesoscale meteorological model, and turbulent components, are generated with the aid of schemes such as a Markov chain scheme or a fully random walk scheme. Examples of such models are described in Uliasz (1994) and Lamb (1979).

A third approach is to use an Eulerian diffusion model, which starts from the mass continuity equation. A first-order closure model for complex terrain was used by Segal et al. (1982) to study dispersion in the Greater Chesapeake Bay area. Enger (1986) has shown the capability of a second-order closure dispersion model in simulating observed dispersion features in a convective boundary layer. The model was also used to simulate dispersion in complex terrain in Enger (1990b) and Enger and Koracin (1995). The present model is a further development of this model. The present model solves prognostically the mean concentration, C, and the second order moments, which include concentration, i.e. $\overline{u'c'}$, $\overline{v'c'}$, $\overline{w'c'}$ and $\overline{c'\theta'}$. In the two-dimensional version of the model used in Enger (1986), the equations for the horizontal fluxes ($\overline{u'c'}$ and $\overline{v'c'}$) were neglected. In Enger (1990b) a three-dimensional version of the model was used. In that version all tendency equations for the second-order moments were included, but with the horizontal advection terms and the horizontal transport terms neglected. Close to the source, these terms have been shown to be as important as other terms in the equations (Fackrell and Robins, 1982). In Enger (1990b) these terms were neglected by supposing the horizontal advection and horizontal dispersion balanced each other. The aim of the present study is therefore to examine the importance of these terms for dispersion in a convective boundary layer.

The basic equations and parameterizations used in the dispersion model are presented in section two and three. The experiments are presented in section four. The model validation is discussed in section five and the sensitivity tests in section six. Conclusions from the present study are given in section seven.

2.2. The basic model equations

The present model is an Eulerian diffusion model, which starts from the mass continuity equation that in tensor notation reads

$$\frac{\partial C}{\partial t} = -U_j \frac{\partial C}{\partial x_j} - \frac{\partial \overline{u'_j c'}}{\partial x_j} + S_c \qquad (1)$$

For explanation of symbols see nomenclature. The corresponding equations for the turbulent fluxes, if we neglect molecular terms and the effect of the Coriolis force on the covariances, are

$$\frac{\partial \overline{u'_i c'}}{\partial t} = -U_j \frac{\partial \overline{u'_i c'}}{\partial x_j} - \overline{u'_i u'_j} \frac{\partial C}{\partial x_j} - \overline{u'_j c'} \frac{\partial U_i}{\partial x_j} - \frac{\partial \overline{u'_i u'_j c'}}{\partial x_j} - \frac{1}{\rho_0} \overline{c' \frac{\partial p'}{\partial x_i}} - \frac{g_i}{\Theta_0} \overline{\theta' c'} \qquad (2)$$

The equation for the covariance, $\overline{c'\theta'}$, is

$$\frac{\partial \overline{c'\theta'}}{\partial t} = -U_j \frac{\partial \overline{c'\theta'}}{\partial x_j} - \overline{u'_j \theta'} \frac{\partial C}{\partial x_j} - \overline{u'_j c'} \frac{\partial \Theta}{\partial x_j} - \frac{\partial \overline{u'_j c'\theta'}}{\partial x_j} - D \qquad (3)$$

The pressure covariance terms in equation (2) are parameterized according to Enger (1986) as

$$\frac{1}{\rho_0} \overline{c' \frac{\partial p'}{\partial x_i}} = \alpha_1 \frac{q}{\lambda} \overline{u'_i c'} - \frac{1}{3} \frac{g_i}{\theta_0} \overline{c'\theta'}, \qquad (4)$$

where α_1 is a constant, and λ is a master turbulent length scale.

In the model version used in Enger (1986) – a 2-dimensional version - the horizontal transport terms were neglected, and in Enger (1990b) the advection terms were also neglected in the equations for the horizontal fluxes. According to measurements by Fackrell and Robins (1982) these terms are as important as other terms, close to the source. Therefore, in the present model the terms are retained and the consequence of neglecting any of the terms shall be discussed in the sensitivity tests.

The vertical transport term is parameterized by use of a gradient diffusion approximation, according to Donaldson (1973) and Mellor (1973), as

$$\frac{\partial \overline{w' u_j' c'}}{\partial z} = -\beta_z \frac{\partial}{\partial z} q\lambda \frac{\partial \overline{u_j' c'}}{\partial z} \tag{5a}$$

and the horizontal transport term is parameterized, in the same manner, as

$$\frac{\partial \overline{u_i' u_j' c'}}{\partial x_i} = -\beta_H \frac{\partial}{\partial x_i} q\lambda \frac{\partial \overline{u_j' c'}}{\partial x_i} \qquad \text{i=1,2} \tag{5b}$$

where β_z and β_H are constants, which shall be determined later. Moreover we treat the transport terms in the equation for the covariance $\overline{c'\theta'}$ in a similar fashion, i.e.

$$\frac{\partial \overline{w' c' \theta'}}{\partial z} = -\beta_z \frac{\partial}{\partial z} q\lambda \frac{\partial \overline{c'\theta'}}{\partial z} \quad ; \quad \frac{\partial \overline{u_i' c' \theta'}}{\partial x_i} = -\beta_H \frac{\partial}{\partial x_i} q\lambda \frac{\partial \overline{c'\theta'}}{\partial x_i} \quad , \qquad \text{i=1,2} \tag{6}$$

The molecular destruction term D is parameterized according to Lumley (1975) as

$$D = \alpha_2 \frac{q}{\lambda} \overline{c'\theta'} \tag{7}$$

where α_2 is a constant.

The values for the constants, α_1, α_2, β_z and β_H are 0.3465, 0.144, 0.36 and 0.36, respectively. The formulation of the master length scale, λ, is given in the Appendix B. The atmospheric variables are obtained from the higher-order closure mesoscale model developed at the Meteorological Institute of Uppsala University, the MIUU mesoscale model. The full description of the model is not repeated here, but the main three-dimensional equations are listed in the Appendix A.

2.3 Numerical method and boundary conditions

A finite-difference numerical method is used to solve the set of dispersion equations. The model uses an expanding telescoping grid mesh with its origin at the source. This means that we get a denser grid mesh near the source where the plume is narrower than further downstream. In all experiments in the study we used 71 x 71 grid points in the horizontal and 31 grid points in the vertical. A grid mesh distance of 50m x 50m x 10m at the source and a model dimension of 50 km x 10 km x 5 km are used. The prognostic equations in the dispersion model are solved by using an advection scheme that is of third-order both in space and time (Enger and Grisogono, 1997). The diffusion is solved with a semi-implicit scheme with weight 0.75 on the future time step. The Arakawa staggered C-grid is used for the model structure. The following boundary conditions are applied at the top of the model

$$\frac{\partial C}{\partial z} = \frac{\partial \overline{w' c'}}{\partial z} = \overline{u' c'} = \overline{v' c'} = \overline{c'\theta'} = 0 \tag{8}$$

and the following are applied at the surface

$$\frac{\partial C}{\partial z} = \overline{w'c'} = \frac{\partial \overline{u'c'}}{\partial z} = \frac{\partial \overline{v'c'}}{\partial z} = \frac{\partial \overline{c'\theta'}}{\partial z} = 0 \qquad (9)$$

2.4 Experiments

Various experiments were designed with the aim at validating and investigating the sensitivity of the dispersion model. The one-dimensional version of the MIUU model was used to simulate an ideal convective boundary layer (CBL). Figure 1 shows the profiles of some of the atmospheric parameters in the simulated CBL. These atmospheric variables were spread into the 3-dimensional dispersion model to obtain a horizontally homogeneous CBL in the model. The boundary layer depth obtained, as the height with the minimum heat flux, is about 846 m, see Figure 1d. Since we intend to compare the model results with those of the Deardorff and Willis (1975), and Willis and Deardorff (1978, 1981) tank experiments, we need, according to Deardorff and Willis (1975), to ensure that the simulated CBL satisfies the criteria $1.5w_* < U < 6w_*$. From Figure 1 we can see that the mean wind is about 2.3 m s^{-1} in the CBL. The convective velocity scale is 1.1 m s^{-1}, hence the criteria is satisfied. With this atmospheric condition a CONTROL experiment was carried out with the full version of the model for validations. A series of other experiments were also carried out to investigate the model sensitivity to some of the terms in equation (2) and (3). The model set-up for each of these sensitivity tests will be discussed later.

2.5 Model validation

The CONTROL experiment was designed to validate the dispersion model against results from tank experiments for surface and elevated sources. Therefore we will simulate dispersion from point sources at 0.062, 0.25, 0.5 and 0.75 of the boundary layer height. For ease of comparison with laboratory and field experiments, the results are presented in dimensionless form. The dimensionless concentration of pollutants and the dimensionless crosswind-integrated concentration are defined as

$$C_N = \frac{z_i^2 U}{Q} C \qquad \text{and} \qquad C_y = \int_{-\infty}^{\infty} C dy \frac{z_i U}{Q} \text{ ,respectively} \qquad (10)$$

The horizontal y-direction is normal to the mean wind direction along x-direction. The dimensionless downwind distance, crosswind distance and height are expressed as

$$X = \frac{x\, w_*}{z_i U}; \quad Y = \frac{y}{z_i} \text{ and } Z = \frac{z}{z_i} \text{ ,respectively.} \qquad (11)$$

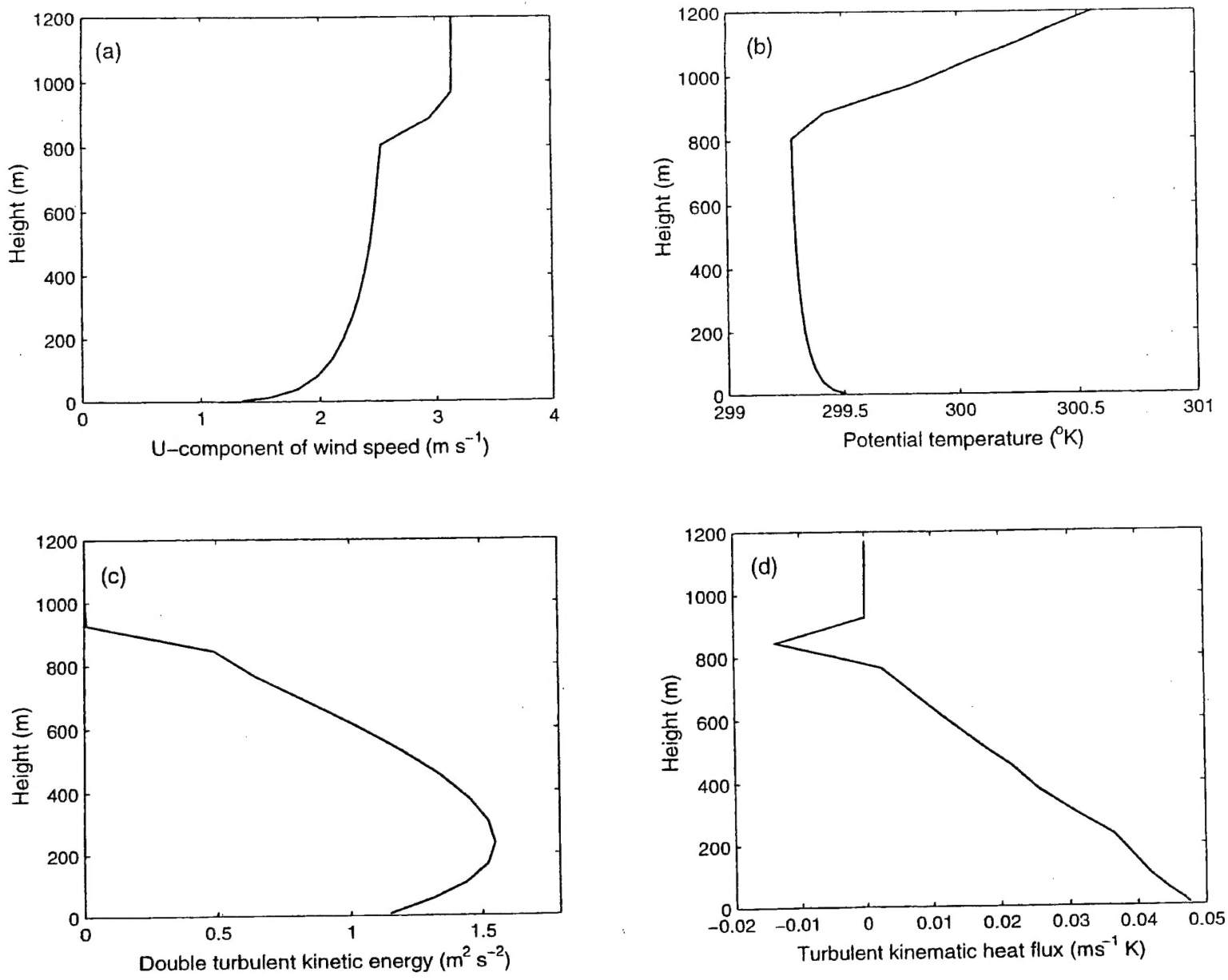

Figure 1. *Vertical profiles of the simulated CBL. (a) U-wind component, (b) Potential temperature (c) Double the turbulent kinetic energy (d) Kinematic turbulent heat flux.*

2.5.1 Crosswind integrated concentration

We start by looking at a vertical cross section of the dimensionless crosswind integrated concentration, C_y, for surface and elevated sources, Figure 2a-d.

For the near ground level release ($0.062z_i$), shown in Figure 2a, the plume centerline first moves horizontally with the surface mean wind then rises rapidly upward (at distance of about 0.4 z_iU/w_*) toward the inversion base as it is being advected by the mean wind. The plume axis reaches an elevated height of 0.9 z_i at distance of around 2.2 z_iU/w_*. It features a surface minimum around 2.2 z_iU/w_*. The plume centerline also starts to descend after striking the inversion layer above to produce a surface maximum concentration at distance 4.5 z_iU/w_*. After a distance of about 6 z_iU/w_* the pollutants are well mixed throughout the entire boundary layer with a dimensionless concentration of about 0.9, which means that 10% has entered the stable boundary layer above. The main behaviors are similar to those in the results from the tank experiment presented in Deardorff and Willis (1975) and the Eulerian model results in Enger (1986). In the tank experiment results the plume centerline started to rise at 0.5 z_iU/w_* to an elevated maximum, which is located roughly at the height 0.8 z_i and at a distance of 1.5 z_iU/w_*. The surface minimum concentration is located around 1.6 z_iU/w_*. In the Enger (1986) results, the elevated maximum is located at height 0.85 z_i at a distance of 2.5 z_iU/w_* and the minimum being located at 1.6 z_iU/w_*.

The result for a source at 0.25 z_i is given in Figure 2b. The plume has a tendency to split into two parts, one rising and the other one descending. The descending part intersects the ground at a distance of about 0.5 z_iU/w_*, after which it rises to merge with the first part. The plume then moves towards the inversion base. The plume reaches its maximum height 0.9 z_i at a downwind distance of 2.0 z_iU/w_*. There are three maximum concentration features in this case; two at the surface, located at distances 0.5 z_iU/w_* and 4.5 z_iU/w_*; the third is an elevated maximum located below the inversion layer at a downwind distance of about 2.0 z_iU/w_*. After a distance of 6 z_iU/w_*, the concentration is well mixed within the entire CBL with concentrations of about 0.95. The results are in very good agreement with those from the tank experiments by Willis and Deardorff (1978), the Lagrangian model simulation by Lamb (1978) and the Eulerian model simulation by Enger (1986). In their results, the plume central line intercepts the ground at 0.4, 0.6, and 0.5 z_iU/w_*, respectively. The present model gives almost the same value of both surface and elevated maximum concentration as observed in the tank experiment results. It is also important to note that the model simulates the 'rebound' of the plume at the surface (i.e. the rise of the plume after striking the ground surface) quite well. This feature, which is well captured by the present model (as observed in the tank experiments), was not simulated by the previous Eulerian model version (Enger, 1986).

Figure 2c shows a similar result, but for a source at the middle of the CBL. Like in the previous case with the source at $0.25z_i$, the plume splits into two parts. The descending part intercepts the ground at about 1.0 z_iU/w_*. The interception took place at a downwind

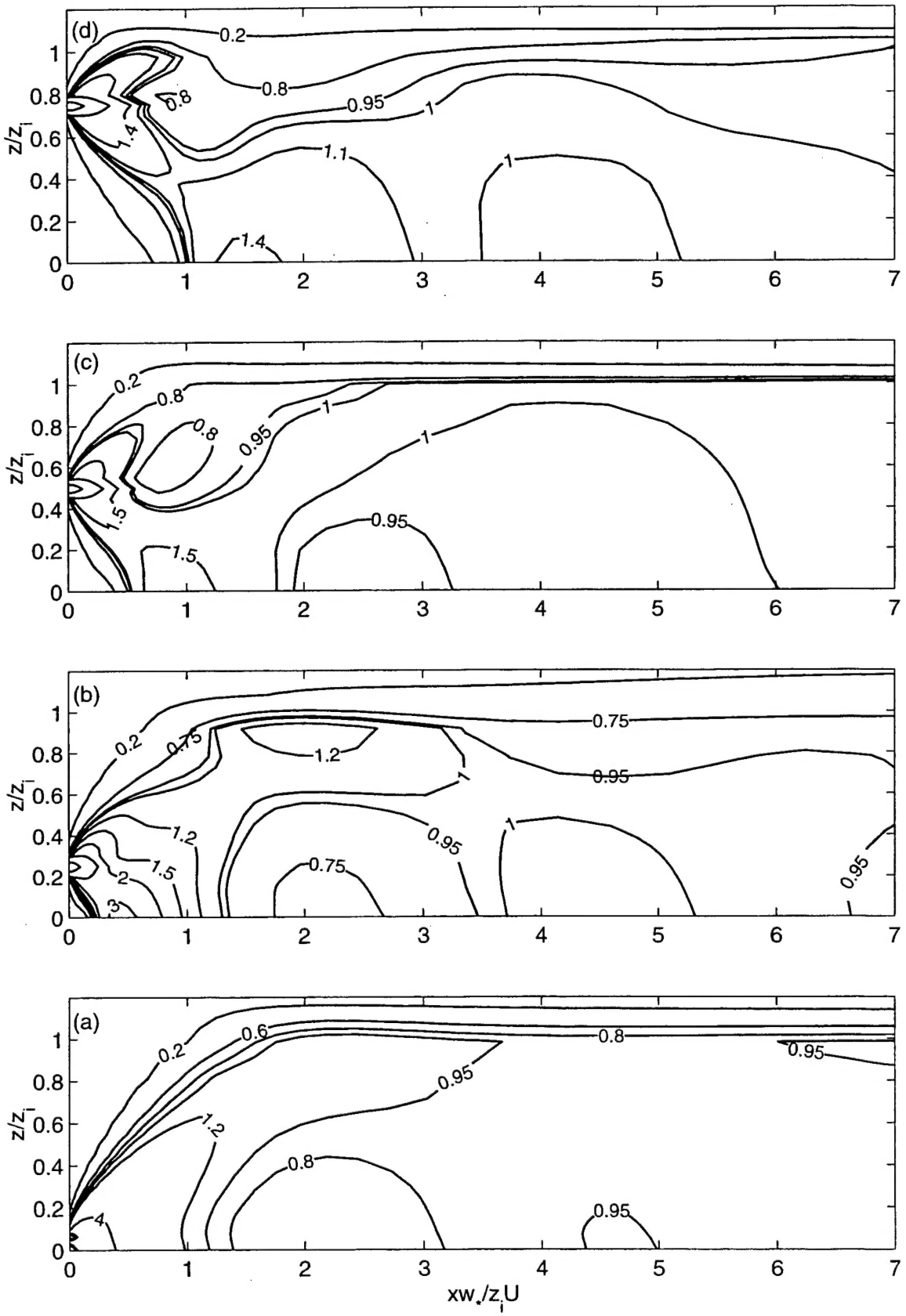

Figure 2. *The dimensionless crosswind integrated concentration for point sources at heights $0.062z_i$ (a), $0.25z_i$ (b), $0.5z_i$ (c) and $0.75z_i$ (d) as simulated in the CONTROL run.*

distance of about 0.8 $z_i U/w_*$ in both the Willis and Deardorff (1981) tank experiment and Lamb's (1982) simulation. We also notice the rising of the plume after intercepting the ground, which is in good agreement with the tank experiment. Another interesting feature is the appearance of a minimum in source height at a distance 0.9 $z_i U/w_*$ downstream. These simulated features, for a source in the middle of the CBL, are in excellent agreement with the CONDOR field experiment results (Moninger et al., 1983) and Willis and Deardorff (1981) tank experiment. The minimum normalized concentration values are 0.75, 0.8, and 0.6 in the present simulation, the tank experiment, and the field experiment, respectively.

For a source at 0.75 z_i, shown in Figure 2d, the descending plume intercepts the ground at a distance of about 1.5 $z_i U/w_*$. This agrees well with Lamb's (1978) simulation, but in the Enger (1986) simulation the intercept took place at 1.9 $z_i U/w_*$. Also in this case, the present model results show a rebound of the plume after intercepting the ground.

Therefore it can be seen that the dimensionless crosswind integrated concentrations from the present model simulations are in excellent agreement with results from the tank experiments, field experiments and Lagrangian model simulations. In some extent the present model simulations give a better representation of these features (i.e. closer to those in the tank experiments) than the simulations of Enger (1986).

Simulated dimensionless crosswind integrated concentrations, C_y, at ground level (for a ground level release at 0.025 z_i) are presented in Figure 3a. These results are compared with the Prairie Grass data (Nieuwstadt, 1980), the results from a water-tank experiment (Deardorff and Willis, 1975) and from Lamb's Lagrangian model simulation (Lamb 1982). From the figure it can be noticed that the present model results agree well with the above-mentioned results, except in the vicinity of the source where the present model diverges from the Prairie Grass data. This is caused by the fact that in the Prairie Grass data the source is located very close to the surface, whereas in the present simulations the source is at 21 m height (z_i = 846m), which results in smaller values of surface concentrations close to the source. There is a minimum of the crosswind integrated concentration at around 2 $z_i U/w_*$. Afterwards it starts to increase and level off to an almost constant value further downstream when the pollutant is well mixed throughout the entire CBL (Convective Boundaary Layer). The minimum corresponds to the minimum concentration at ground for a source at the height 0.062 z_i, shown in Figure 2a.

2.5.2 Mean ground-level concentration

Now let us examine the corresponding dimensionless ground-level concentrations $C_N(x,y,0)$, which are presented in Figure 4. One of the most striking features in this figure is that the surface concentration distribution across the plume is non-Gaussian. This non-Gaussian distribution is especially pronounced for a source at height 0.062 z_i, Figure 4a, where a double maximum across the plume is present. The double maximum appears between a downwind distance of about 0.5 and 2.0 $z_i U/w_*$. This feature is also present in Lamb's (1979) simulations with the Lagrangian model. Such a feature has also observed in some dispersion measurements on the East Coast of the US under CBL conditions

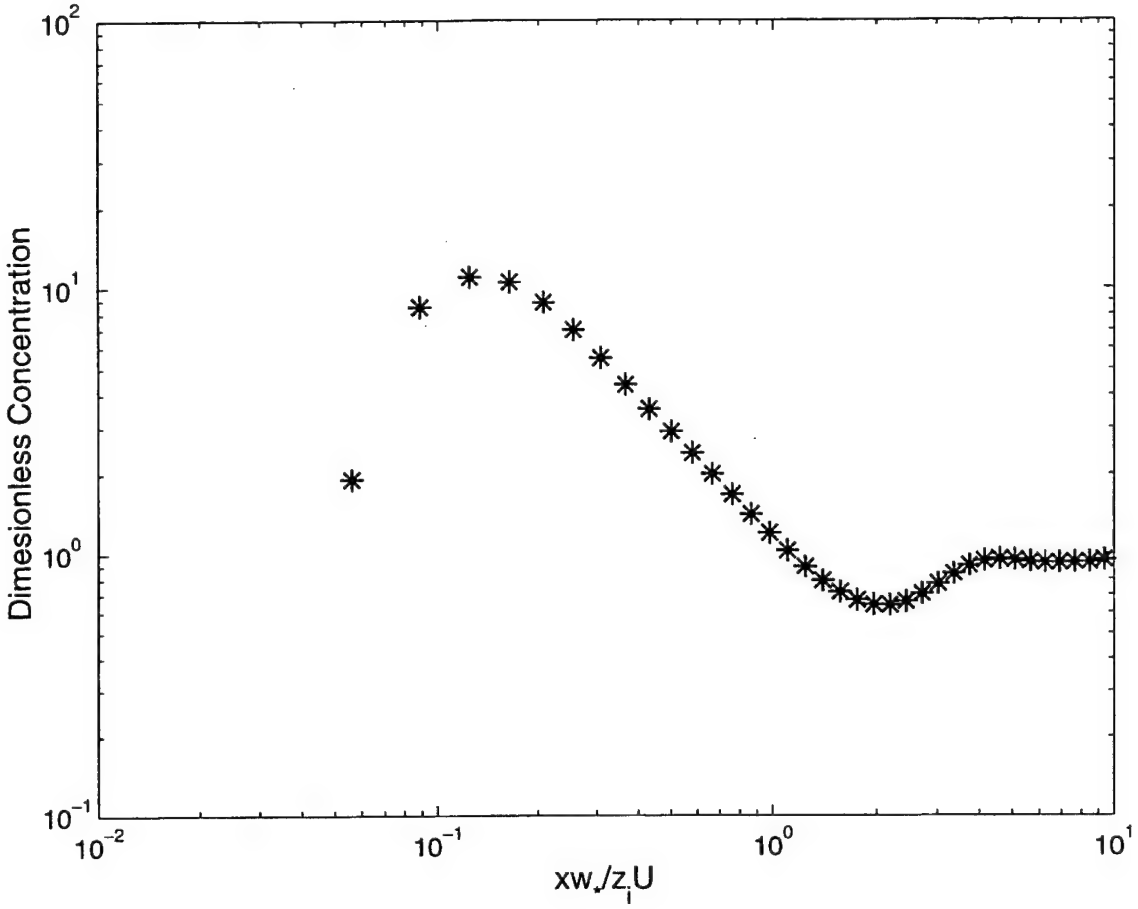

Figure 3. *The dimensionless crosswind integrated concentration at ground level as a function of the dimensionless downwind distance* $x w_*/z_i U$ *for source at height* $0.025\ z_i$.

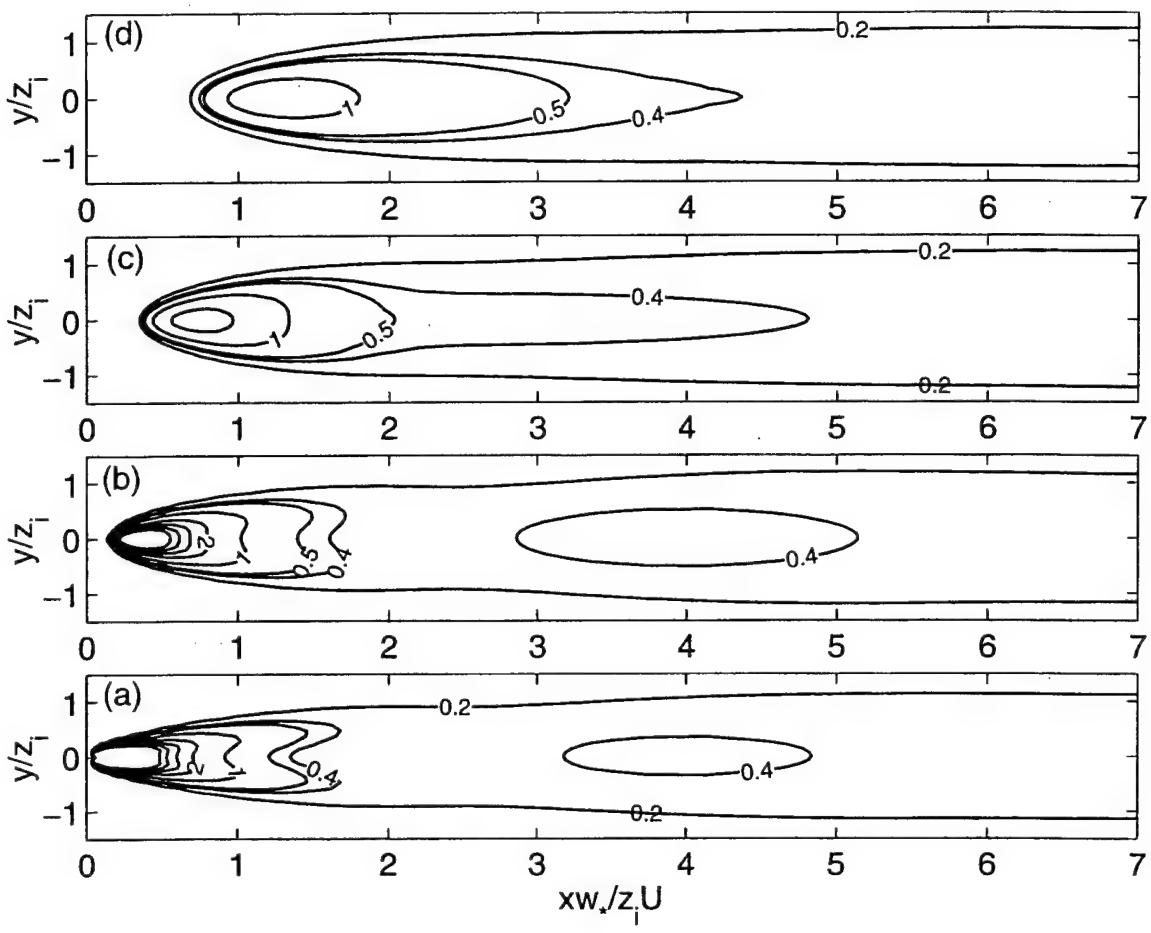

Figure 4. *The dimensionless ground-level concentration in x-y plane for point sources at heights 0.062 z_i (a), 0.25 z_i (b), 0.5 z_i (c) and 0.75 z_i (d).*

(Nappo 2001, personal communication). As will be discussed later in the sensitivity test, advection and horizontal diffusion terms in the equations for the fluxes play a significant role in the creation of this feature. Figure 5 shows the ground level concentration across the plume at a distance of 1.0 $z_i U/w_*$ for source heights $0.062z_i$ and $0.25z_i$. A similar shape, with two maximum features in the ground level concentration, appears for both source heights, but is less pronounced for a source at height $0.25z_i$.

2.6 Sensitivity tests

The explanation for the shown features of dispersion from a point source in the CBL is according to Lamb (1982) that the distributions of the vertical winds are non-Gaussian. Instead there should be short periods – or small areas – with high up-winds in the convective cells, followed by long periods – or large areas – with slow descending air. However, the Eulerian model that has been used here does not include any probability density functions of the vertical velocity, but still gives very similar dispersion distribution from a point source in the CBL. The following sensitivity tests will show that there exists another explanation to the plume behaviour in a CBL. The sensitivity tests will also explain some horizontal features that can be noticed in the simulation results shown above.

The primary aim with the sensitivity tests is to investigate the relative importance of the horizontal advection and diffusion terms in equations (2) and (3). For this purpose a number of sensitivity experiments were carried out with model. In the first, both the advection and diffusion terms are neglected. In the second, only the diffusion terms are neglected, whereas in the third, only the advection terms are excluded. Furthermore, tests have been performed to investigate the sensitivity of the coefficient, $\square_H$, in the diffusion terms.

2.6.1 No Advection, No Horizontal Diffusion Experiment (NOAD)

The experimental set-up for this experiment is the same as for the control experiment, except that both the advection and horizontal diffusion terms in the equation for all the fluxes ($\overline{u_i'c'}$ and $\overline{c'\theta'}$) are excluded. It should be noted that for a steady state solution with no advection and no horizontal diffusion terms in equation (2), the expression for the horizontal crosswind flux, $\overline{v'c'}$, reduces to

$$-\overline{v'c'} = \frac{\lambda}{\alpha_1 q}\overline{v'^2}\frac{\partial C}{\partial y} \equiv K_H \frac{\partial C}{\partial y}$$

In our case, with horizontally homogenous conditions the turbulence is constant at a certain height, giving an exchange coefficient K_H that is constant for that height. A constant K_H (Fickian diffusion) should give a Gaussian-like distribution of concentrations across the plume. In fact, the results of the model for this case show that the horizontal concentration distribution is Gaussian (see Figure 6, circles). Moreover, all the essential dispersion features for a point source in a CBL, i.e. descending, ascending and 'rebound'

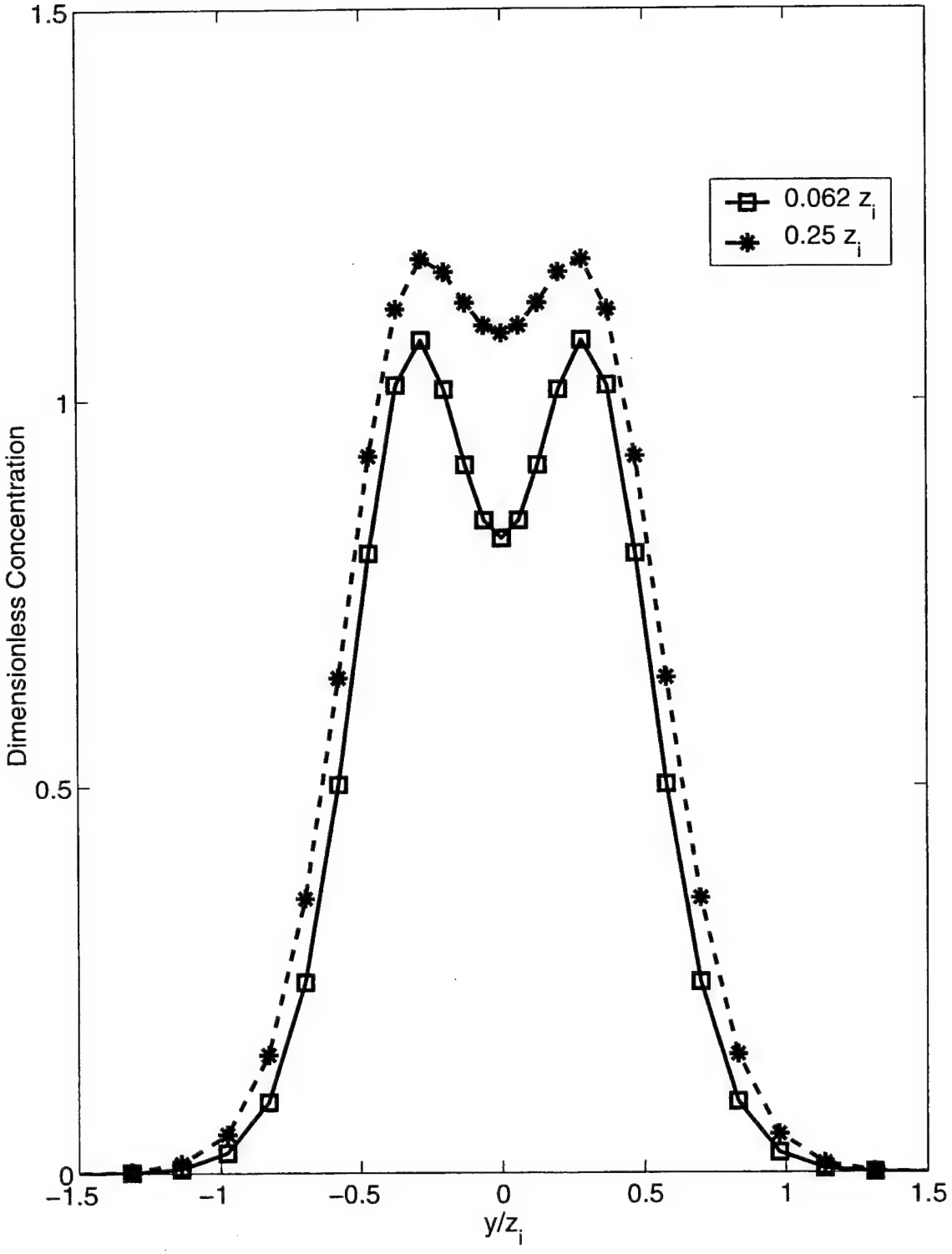

Figure 5. *Lateral crosswind profile of dimensionless ground-level concentration plane for point sources at heights 0.062 z_i (squares) and 0.25 z_i (stars) at 1.0 $z_i U/w_*$ downstream.*

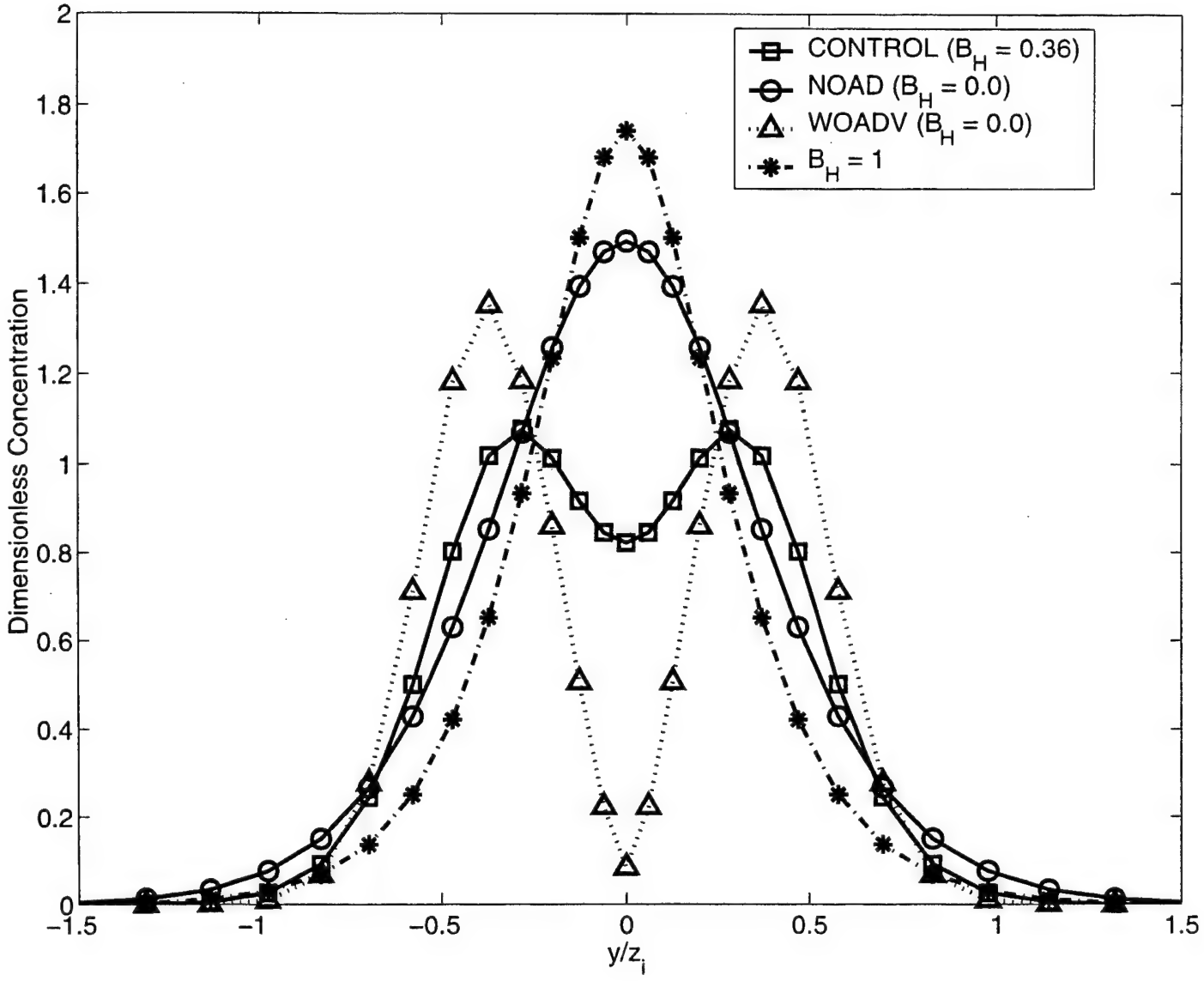

Figure 6. *Comparison of the lateral crosswind profile of the dimensionless ground-level concentration. Source height $0.062z_i$ and distance $1.0\ z_iU/w_*$.*

of the plume and the non-Gaussian distribution across the plume, disappear. Figure 7 shows the simulated dimensionless crosswind integrated concentration and the dimensionless ground-level concentration as an example of this behavior. Results from this experiment show that the advection and diffusion terms in the equation for $\overline{w'c'}$ are crucial in simulating the vertical distribution of the concentration from a point source in a CBL.

2.6.2 Only Advection Experiment (OADV)

As pointed out by Fackrell and Robins (1982), the advection terms and the diffusion terms are quite large close to the source. They also found that the two terms are almost equal but with opposite sign. Our hypothesis is that the non-Gaussian distribution and splitting of the plume is caused by the fact that the advection term in the equations for the fluxes is larger than the diffusion terms. If we exclude the diffusion term but keep the advection in the equations for the second-order moments, the splitting of the plume should increase considerably. Figure 8a shows examples of this behavior for a ground level source (0.062 z_i). The results are compared with the corresponding results obtained from the CONTROL experiment, Figure 4a. In Figure 6 the ground level concentration values across the plume at distance 0.7 $z_i U/w_*$ are shown for the different runs: control run (squares), NOAD-experiment (circles), OADV-experiment (triangles), and a simulation with higher diffusion (constant $\beta_H = 1$) than in the CONTROL run (stars).

The influence of the advection terms on the dispersion features can be explained by looking at the fluxes. If we have, for example, a Gaussian distribution (like in NOAD experiment) the horizontal crosswind flux is zero at centerline and increases in magnitude outwards to a maximum value, after which it decreases again. This maximum value is of course larger in magnitude closer to the source than further downstream. The advection term does not effect the fluxes at the centerline, as they are zero there, but away from the centerline the advection term causes these higher fluxes closer to the source to move downstream. Which in turn increases the flux value downstream and sharpens the flux gradient from the centerline and out. Larger gradients and larger magnitudes of the fluxes cause an increased movement of concentration out from the centerline, which causes the plume to split. The advection of fluxes also explains the noticed distribution of concentration in the vertical direction, with a plume that split into an ascending and a descending part.

2.6.3 Only Diffusion Experiment (ODIF)

The model set up for this experiment is the same as for the NOAD experiment, except that the diffusion terms are included equation (2) and (3). The model results replicate those of the NOAD experiment, where the CBL features are absent and the lateral crosswind concentration profile is more Gaussian-like. The diffusion terms in the second order moment equations act to smooth out the gradients of the fluxes, which means that the diffusion terms act in the opposite direction of the advection terms. If the advection term is larger than the diffusion term the plume can split both horizontally and vertically as shown in the CONTROL run.

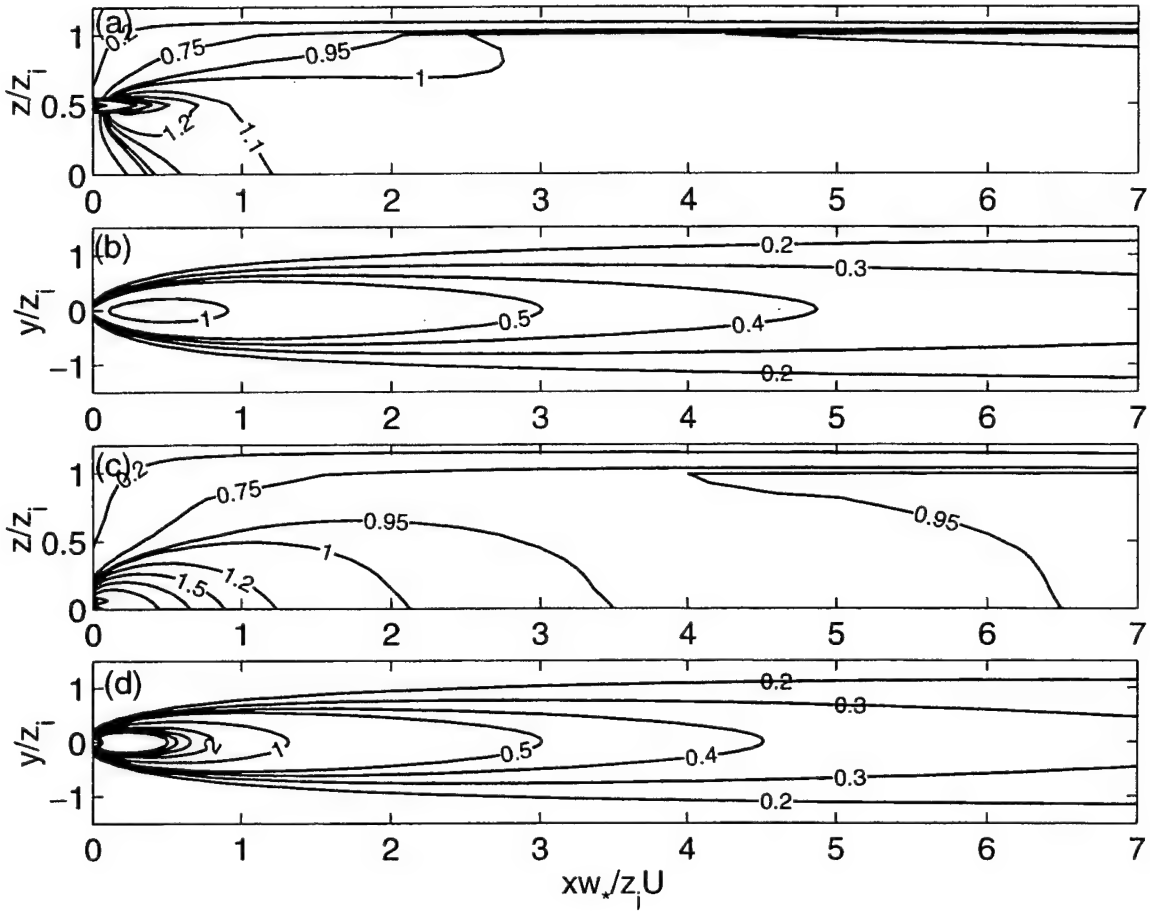

Figure 7. *The model results from NOAD experiment for point source at height 0.5 z_i. (a) the dimensionless crosswind integrated concentration and (b) the dimensionless ground-level concentration and for a point source at height 0.062 z_i. (c) the dimensionless crosswind integrated concentration and (d) the dimensionless ground-level concentration source at height 0.5 z_i.*

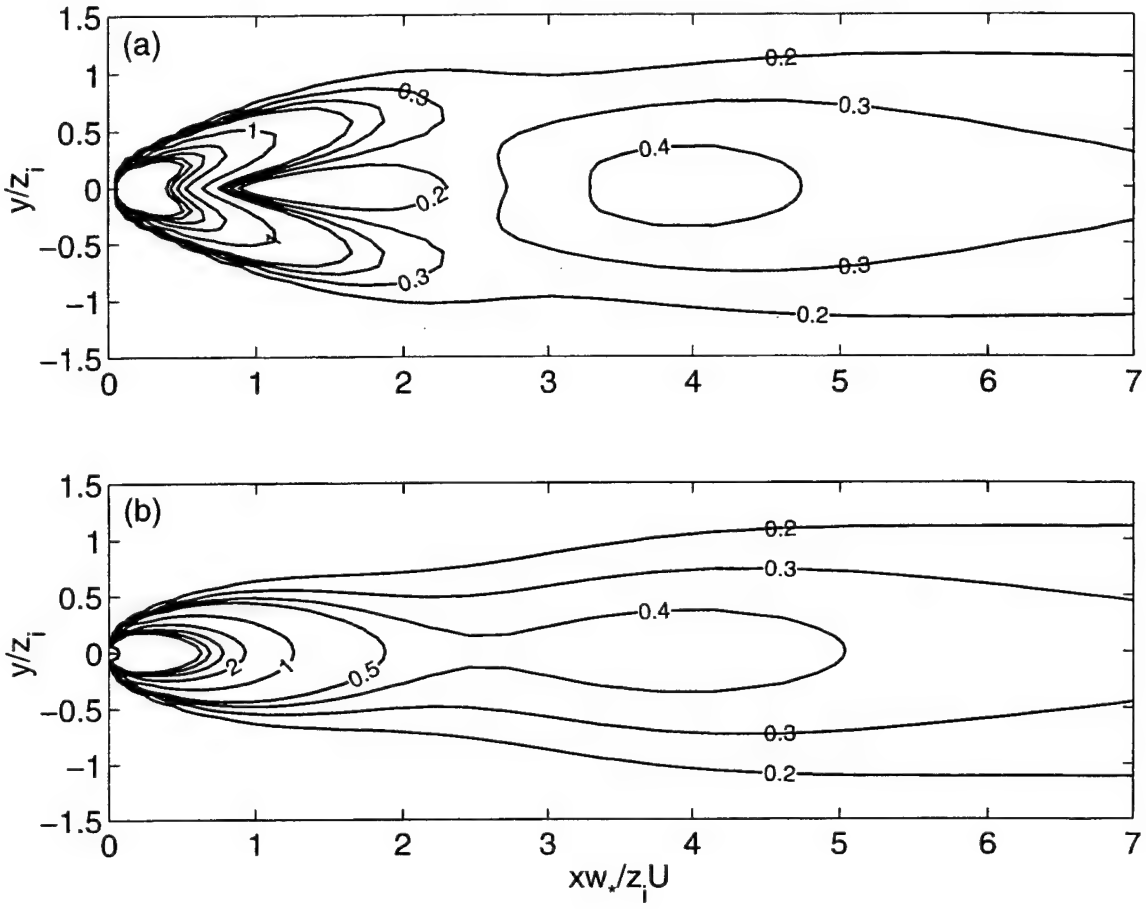

Figure 8. *(a) Dimensionless ground-level concentration for a point source at height 0.062 z_i as simulated in WOADV experiment (b) dimensionless ground-level concentration for a point source at height 0.062 z_i as simulated in control run but with $\beta_H = 1$.*

2.6.4 Effect of Horizontal Diffusion Coefficient, β_H

This experiment was designed to investigate the effect of the diffusion coefficient, β_H, on the model simulations. The model set-up is the same as in the CONTROL experiment except that $\beta_H = 1$, which means a much larger diffusion of the fluxes. The results show the same features as the CONTROL experiment but without the horizontal splitting of the plume, see figure 8b. The constant $\beta_H = 1$ causes less concentration to move out from the centerline resulting in a narrower plume and higher concentration in the center (see Figure 6). The model constant $\beta_H = 0.36$, used in the CONTROL run was chosen to be equal to the vertical constant β_z, as the main turbulence features are caused by eddies going through the whole CBL and the time scales (and length scales) should be the same vertically and horizontally.

2.7 Summary and conclusions

A higher order closure dispersion model suitable for the airflow over complex terrain is developed, tested and validated under convective conditions. The study has clearly illustrated that the present higher-order closure dispersion model is capable of modeling dispersion in convective conditions quite realistically. There have been discussions in the literature as to whether a Eulerian diffusion model would enable the prediction of dispersion in a convective boundary layer or not. However, the results from the simulations show very good agreement with Willis and Deardorff's experiments and with Lamb's Lagrangian model. The explanation for the shown features of dispersion from a point source in the CBL is according to Lamb (1982) that the distributions of the vertical winds are non-Gaussian and have a negative mode in the CBL and that the probability density profiles change with height. However, the Eulerian model that has been used here does not include any probability density functions of the vertical velocity, but still gives very similar dispersion distribution from a point source in the CBL. The sensitivity tests performed showed that there exists another explanation to the plume behavior in a CBL.

Sensitivity studies with the model helped to identify the role the advection and diffusion terms in the equations for fluxes play in simulating the dispersion from point sources in CBLs. To simulate the horizontal and vertical features in the CBL, the advection terms in the equations for the second order moments that involve concentration are shown to be very important. The horizontal concentration as well as the vertical concentration distribution are sensitive to the balance between the advection and diffusion terms in the second order moment equations.

The main findings in the present paper are:

- The descending and ascending of a plume in a convective boundary layer is caused by the advection of the vertical concentration flux, $\overline{w'c'}$.

- The advection of the horizontal fluxes, $\overline{v'c'}$ and $\overline{u'c'}$, causes the plume to split horizontally.

- The diffusion terms in the equations for the fluxes act in the opposite direction of the advection terms, but the advection and diffusion terms do not balance each other completely in the CBL.

3. Development, validation and comparison of a higher-order closure mesoscale model

3.1 Comparison of meteorological fields from MIUU and MM5

3.1.1 Introduction

Dispersion models need realistic three-dimensional atmospheric fields as input for transport and dispersion studies of atmospheric pollutants. In this study, data from the extensive field program, MOHAVE (Measurements Of Haze And Visibility Experiment) (e.g. Green, 1999; Pitchford et al., 1999), have been used to evaluate the meteorological output of two atmospheric mesoscale models: the Meteorological Institute of Uppsala University's model (MIUU model) and the Fifth-Generation Penn State/NCAR Mesoscale Model (MM5).

Project MOHAVE was conducted in the southwestern United States (see Figure 9) and included meteorological, chemical and visibility measurements at several stations. Upper-air observations were made at several sites using radiosondes, wind profilers and a radio acoustic sounding system (RASS). The main goal of project MOHAVE was to assess the effects of the Mohave Power Plant (MOPP), a large coal-fired power plant in the Colorado River Valley in southern Nevada, circa 120 km to the south-southeast of Las Vegas, on visibility in the southwestern United States, in particular at Grand Canyon national park (Green, 1999).

3.1.2 Model Description

The MIUU model is a higher-order turbulence closure model of level 2.5 (according to Mellor and Yamada, 1974). It applies a terrain-following coordinate system (Pielke, 1984), is hydrostatic, and includes prognostic equations for the mean variables and turbulent kinetic energy (e.g., Enger et al., 1993). The turbulence closure scheme was corrected to include wall effects in the redistribution terms for the second-order moments (Andrén, 1990) in order to account for the influence of the underlying surface. Andrén (1990) pointed out that this is of importance particularly for air pollution applications. Additionally, the model includes routines for clouds, radiation and soil surface temperature and humidity. The model output, i.e., the velocity, temperature and turbulent kinetic energy fields, is then used in the dispersion model (see Section 3.2) together with the turbulent length scale, to compute all the second-order moments, that are required in the prognostic equations for the atmospheric pollutant or tracer concentrations (Andrén, 1990).

A new lateral boundary condition, based on a modified version of Davies (1976) flow relaxation scheme, is used in the model to introduce the large-scale synoptic fields from the NCEP/NCAR Reanalysis project (Kalnay et al., 1996). A terrain-following flow

relaxation parameter is applied in order to allow mesoscale phenomena in the planetary boundary layer to develop in the vicinity of the lateral boundaries. Therefore, the flow-relaxation parameter K (according to Davies, 1976) is chosen to be zero at the ground surface and approaching its maximum value of 0.0015 at 500 meters above ground level (AGL) for the horizontal wind components, and 4000 meters AGL for temperature and humidity. Between these heights and the model top, the parameter K is set to 0.0015. Between ground level and 500 meters AGL, or 4000 meters AGL, respectively, a linear interpolation is used for the parameter K. The function F (according to Davies, 1976) was chosen to be zero everywhere, and no relaxation was applied for the vertical wind component. The pressure fields of the NCEP/NCAR Reanalysis project were interpolated to the model grid points to obtain the large-scale synoptic pressure gradient forces.

Since Reanalysis data were available only every six hours, the large-scale synoptic pressure, temperature, humidity, and velocity fields were interpolated linearly in between these times. The method allowed the model to run for more than 9 days, without experiencing any instability.

The MM5 mesoscale model is well-known and thoroughly described in Grell et al. (1995). A detailed description is omitted here for brevity reasons.

3.1.3 Model Simulations

The MIUU model was run from 5 Standard Mountain Time (SMT = UTC –7 hours) on August 5, 1992, to 5 SMT on August 14, 1992. NCEP/NCAR Reanalysis data have been used to prescribe the large-scale synoptic pressure-fields and to update the boundary values of the mesoscale model using the method described above. Surface elevation and land-use information have been obtained from the International Geosphere-Biosphere Program Data and Information System (Belward, 1996). Total cloudiness was set to 0.1 during the entire period and 5 K were added to the NCEP/NCAR Reanalysis temperatures, to get a better agreement with measurements. The model was run with 30 vertical levels, and without using any cloud routines.

MM5 model simulations for MOHAVE have been performed and described by Isakov (1998). A brief description of the simulations can be found in Koracin et al. (2000). MM5 was run from 17 SMT on August 5, 1992, to 16 SMT on August 14, 1992. MM5 preprocessing includes an advanced objective analysis of the synoptic data from the global network, providing detailed initial and boundary conditions for the simulations. A non-hydrostatic version with 35 vertical levels was used. To include more upper-air observations in the initialization process, an expanded grid of 60 km beyond the lateral boundaries of the model was used for the preprocessing.

In both models, a horizontal resolution of 3 km was used. The model domain covered the area between 34.5° and 37° North and 112° to 116° West (see Figure 9). For the MM5 runs, terrain was obtained from a 30'' Defense Mapping Agency Database, and then considerably smoothed. The terrain used in the MM5 simulations does not exactly correspond to Figure 9.

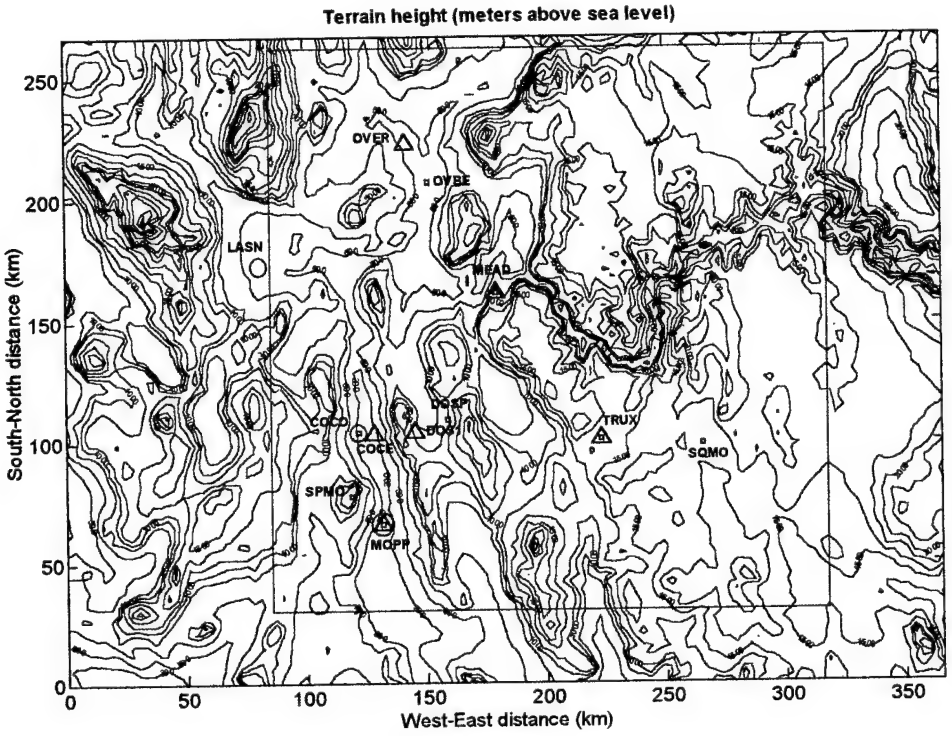

Figure 9. *Model domain as used for MIUU-model simulations. The total domain is used for the atmospheric model simulations, the inner square is used for the dispersion-model simulations. Stations are as follows: MOPP = Mohave Power Plant (213 m ASL); COCO = Cottonwood Cove, West (274 m ASL); COCE = Cottonwood Cove, East (201 m ASL); DOSP = Dolan Springs (853 m ASL); DOS1 = Dolan Springs, Tab (1015 m ASL); MEAD = Meadview (905 m ASL); OVER = Overton (424 m ASL); OVBE = Overton Beach (396 m ASL); SPMO = Spirit Mountain (1498 m ASL); SQMO = Squaw Mountain (1981 m ASL); TRUX = Truxton (1350 m ASL) and LASN = Las Vegas McCarran International Airport (664 m ASL). Circles indicate meteorological surface observations, triangles meteorological upper-air observations and squares tracer measurements. For details and coordinates see Pitchford et al. (1999).*

3.1.4 Model Results

Results from both models show that the strong channeling, exerted on the flow by the Colorado River valley, with heights of about 200 – 300 m ASL at the bottom of the valley and ridges of up to 1800 m ASL on both sides of the valley, is dominating most of the time. Since the valley axis is roughly south to north, the flow in the valley is usually to the South in winter and to the North in summer (e.g., Green, 1999). Figure 10 shows an example of the flow pattern at 140 m ASL obtained with the MIUU model.

Enger et al. (1993) found, when studying the flow regime of this part of the Colorado River valley, that the wind veering simulated over the range of topographic elevations is often larger than 100 degrees, in some cases as large as 180 degrees. This was also seen in the results of both models and in the measurements.

3.1.5 Comparison and Statistical Evaluation against Surface and Upper Air Measurements

Figure 11 shows a comparison of MIUU and MM5 model results against surface measurements at Mohave Power Plant (MOPP). In both models, the agreement between measured and modeled wind speed is quite poor. Both measured and simulated wind directions clearly show the channeling effect of the Colorado River valley. The model simulated wind direction fields are compared poorly against the measurements during larger time periods. However, the MIUU model seems to perform slightly better for temperature, whereas for humidity, MM5 gives slightly better results.

Table 1. *Root mean square differences of MM5 and MIUU model simulations compared to upper-air observations at stations MOPP, COCE, DOS1, MEAD, OVER and TRUX. Stations are indicated by triangles in Figure 9. Number of profiles is indicated as $N_{Profiles}$. W indicates comparison to wind-profiler data, RS comparison to radio soundings. All differences are calculated as the mean for the entire height interval of the profiles, mostly from ground surface up to 5000 m AGL.*

		Root Mean Square Differences: MM5					**Root Mean Square Differences: MIUU**				
	$N_{Profiles}$	Vector (m/s)	U (m/s)	V (m/s)	T (K)	Q (g/kg)	Vector (m/s)	U (m/s)	V (m/s)	T (K)	Q (g/kg)
MOPP	205 W	3.3	3.6	4.2	8.8*	-	3.1	3.5	4.5	10.8*	-
COCE	25 RS	3.3	2.7	3.4	2.3	3.0	3.2	2.5	4.0	2.0	3.1
DOS1	17 RS	2.7	2.8	3.1	2.3	1.6	2.4	2.5	2.9	3.7	2.0
MEAD	205 W	3.2	3.2	4.4	-	-	3.1	3.0	3.8	-	-
OVER	177 W	3.4	2.5	4.6	-	-	3.6	2.1	5.1	-	-
TRUX	205 W	3.2	3.3	4.7	-	-	2.8	3.5	3.7	-	-

* Comparison with RASS measurements of doubtful quality. Height interval: 100 – 1300 m AGL.

Table 1 shows a comparison of the model-simulated data with upper-air measurements. Only the time period where results from both models were available was chosen for the comparison. Root mean square (RMS) differences (e.g. Pielke, 1984) were calculated using all available upper-air data. RMS differences were calculated as the mean over the entire height interval of the respective profile at each station. Finally, the mean of the

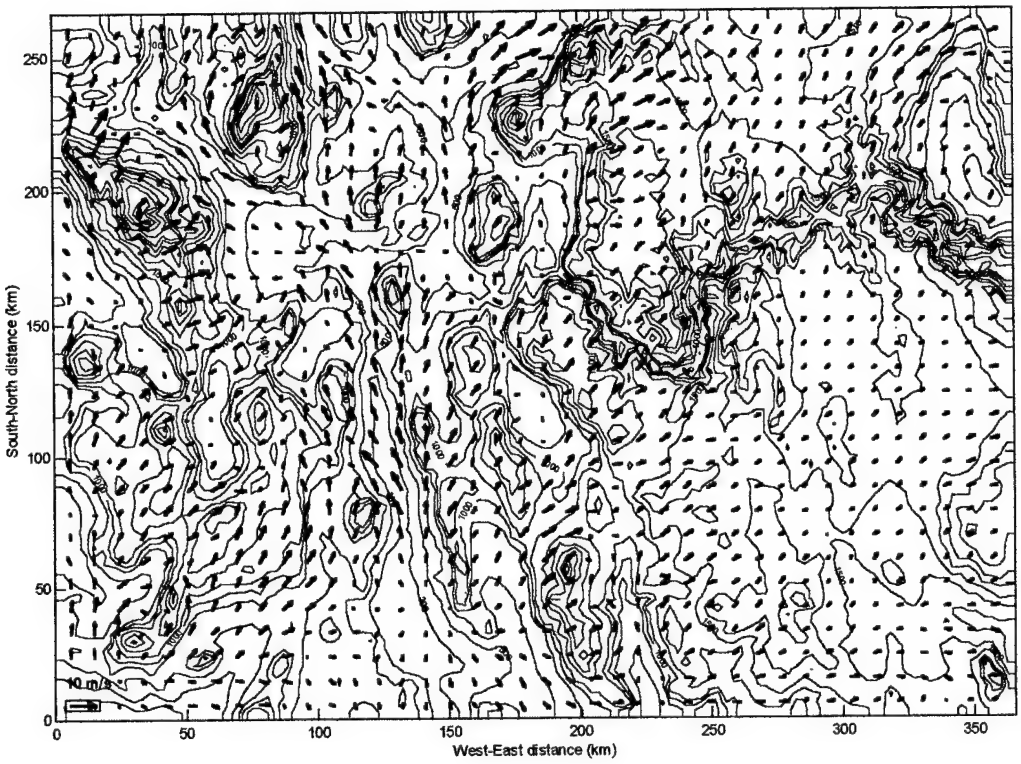

Figure 10. *Horizontal wind vectors at 140 m AGL as simulated by the MIUU model at 12 SMT on August 5, 1992. A scaling arrow of 10 m/s is drawn in the lower left corner.*

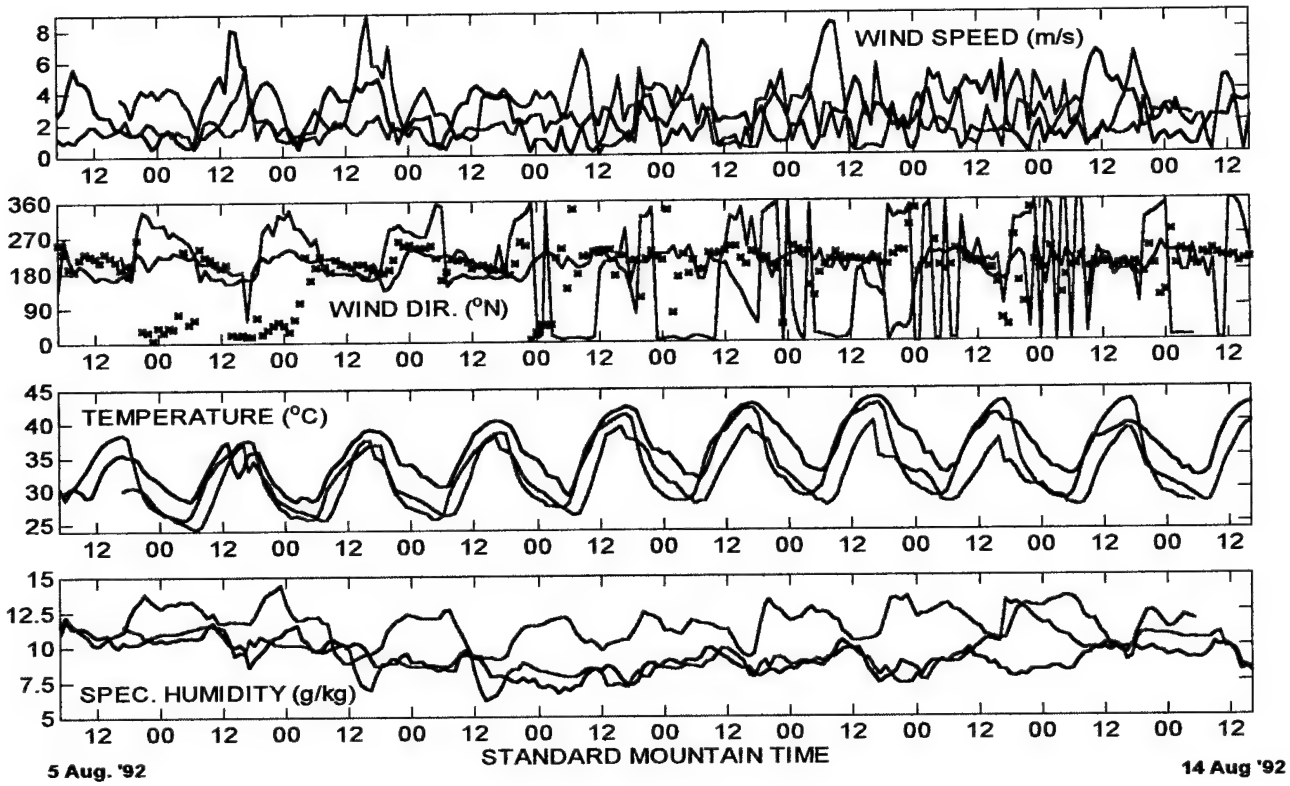

Figure 11. *Comparison of model results with surface measurements at MOPP. Black lines/croses indicate measurements, blue lines MIUU model results and red lines MM5 model results. The grid-point closest to MOPP is used for the model comparison.*

RMS differences of all available profiles at one station was calculated and included in Table 1. The number of profiles used is given as $N_{Profiles}$ in the table. As can be seen from the table, both models perform comparatively equally, giving a RMS difference of slightly over 3 m/s for the vector, around 3 m/s for the u-wind and around 4 m/s for the v-wind RMS differences. The comparison with RASS measurements (indicated by asterisks in the table), however, should not be taken seriously, since the quality of these measurements seems to be rather poor.

3.1.6 Conclusions

Two mesoscale models, the MIUU model and the MM5 model, have been compared to surface and upper-air observations. Statistical methods give an insufficient answer to the question, which model actually is performing better. Thus, as Koracin et al. (2000) suggested, tracer measurements should be used to evaluate wind fields from different models. Studies, using both MIUU and MM5 model results as input to a higher-order closure dispersion model, will be presented in Section 3.2.

3.2 Dispersion comparisons between models

3.2.1 Introduction

Many of our air-quality related problems are concerned with pollutant transport and diffusion in complex terrain. However, modeling pollutant dispersion in such areas is a difficult task because of the associated complex flow and turbulence. The conventional Gaussian and Eulerian K-theory models are inadequate for modeling dispersion in complex terrain. Alternatively, Lagrangian particle models and higher-order closure models are usually used for this purpose, e.g. Yamada (1985) and Enger and Koracin (1995).

This section reports a higher-order closure dispersion (HOCD) model, suitable for modeling dispersion in complex terrain. A brief description of the model is presented in 3.2.2. The model has been applied to simulate dispersion in a convective boundary layer (CBL). Comparison of the results with those from tank experiments is done in 3.2.3. The model has also been used to simulate tracer transport and dispersion in the complex terrain, discussed in Section 3.1. The model results are compared with available measurements in 3.2.4.

3.2.2 Model Description

The present model is an Eulerian diffusion model, which starts from the mass continuity equation

$$\frac{\partial C}{\partial t} = -U_j \frac{\partial C}{\partial x_j} - \frac{\partial \overline{u'_j c'}}{\partial x_j} + S \qquad (1)$$

The corresponding equations for the turbulent fluxes, if we neglect molecular terms and the effect of Coriolis forces on the covariance, are

$$\frac{\partial \overline{u'_i c'}}{\partial t} = -U_j \frac{\partial \overline{u'_i c'}}{\partial x_j} - \overline{u'_i u'_j} \frac{\partial C}{\partial x_j} - \overline{u'_j c'} \frac{\partial U_j}{\partial x_j} - \frac{\partial \overline{u'_i u'_j c'}}{\partial x_j} - \frac{1}{\rho_0} c' \overline{\frac{\partial p'}{\partial x_i}} - \frac{g_i}{\Theta_0} \overline{\theta' c'} \quad (2)$$

The equation for the covariance, $\overline{c'\theta'}$, is

$$\frac{\partial \overline{c'\theta'}}{\partial t} = -U_j \frac{\partial \overline{c'\theta'}}{\partial x_j} - \overline{u'_j \theta'} \frac{\partial C}{\partial x_j} - \overline{u'_j c'} \frac{\partial \Theta}{\partial x_j} - \frac{\partial \overline{u'_j c'\theta'}}{\partial x_j} - D \quad (3)$$

The pressure covariance terms in equation (2) are parameterized according to Enger (1986) as

$$\frac{1}{\rho} c' \overline{\frac{\partial p'}{\partial x_i}} = \alpha_1 \frac{q}{\lambda} \overline{u'_i c'} - \frac{1}{3} \frac{g_i}{\theta_0} \overline{c'\theta'} \quad (4)$$

where α_1 is a constant, and λ is a master turbulent length scale.

The vertical transport term is parameterized using a gradient diffusion approximation according to Donaldson (1973) and Mellor (1973). The molecular destruction term D is parameterized according to Lumley (1975) as

$$D = \alpha_2 \frac{q}{\lambda} \overline{c'\theta'} \quad (5)$$

The values for the constants, α_1, and α_2, are 0.3465 and 0.144, respectively. The formulations of the master length scale, λ, are described in Enger (1990). A finite-difference numerical method is used to solve the set of model equations. The model uses an expanding telescoping grid mesh with its origin at the source. This means that we get a denser grid mesh near the source, where the plume is narrower than further downstream. The prognostic equations in the dispersion model are solved using a third-order advection scheme, described in Enger and Grisogono (1997). The diffusion is solved with a semi-implicit scheme with weight 0.75 on the future time step. The Arakawa staggered C-grid is used for the model structure. The following boundary conditions are applied at the top of the model:

$$\frac{\partial C}{\partial z} = \frac{\partial \overline{w'c'}}{\partial z} = \overline{u'c'} = \overline{v'c'} = \overline{c'\theta'} = 0 \quad (6)$$

and the following applied at the surface:

$$\frac{\partial C}{\partial z} = \overline{w'c'} = \frac{\partial \overline{u'c'}}{\partial z} = \frac{\partial \overline{v'c'}}{\partial z} = \frac{\partial \overline{c'\theta'}}{\partial z} = 0 \quad (7)$$

3.2.3 *Model Simulations in Horizontally Homogenous CBL*

The model is used to simulate the characteristics of plume dispersion in a CBL with point sources at 0.62, 0.25 and 0.5 of the boundary layer height. A one-dimensional version of the MIUU mesoscale model was used to simulate an ideal CBL used in the dispersion model. The CBL height, obtained as the height of minimum heat flux, is about 846 m, with a mean wind speed of about 2.3 m/s. The convective velocity scale is calculated to 1.1 m/s. The CBL is similar to those used in the Deardorff and Willis tank experiments (Deardorff and Willis, 1975; Willis and Deardorff, 1978, 1981). It satisfies the same criteria, i.e., $1.5w_* < U < 6w_*$.

Contour plots (in the x-z plane) of the dimensionless crosswind integrated concentration, simulated by the model with different source heights are presented in Figure 12. The results are compared with results from the tank experiments. We can see that the simulations show the significant features of dispersion in CBL, as observed in the tank experiments, remarkably well. The model captures the rise and fall of the plume. The 'rebound' of the plume after striking the surface, or the inversion layer above, is equally well simulated. The maximum and minimum concentration values, including their locations, agree very well with the results from the tank experiments.

3.2.4 *Model Simulation in Complex Terrain*

The model was then used to simulate pollutant transport and dispersion at Colorado River valley during the period of an intensive field program, the Measurement of Haze and Visibility Experiment (MOHAVE). The topography of the area with the domain, used in the presented dispersion simulation, is shown in Figure 9. One of the main objectives of the field experiment was to investigate and identify the possible short- and long-term impacts of atmospheric pollutants from major urban areas and industrial sources (especially from Mohave Power Plant, MOPP) on the Grand Canyon and its vicinity. In the field experiment, PTF ortho-perfluordimethylcyclohexane (oPDCH) was released continuously from MOPP during 50 days in summer. Forty-five percent of the oPDCH consists of the isomer ortho-cis (oc)PDCH, which was measured at the receptor sites. The tracers are inert, non-depositing, and non-toxic chemicals. The stack height of the power plant is 150 m. The effective source height is calculated to be about 300 m AGL. Thus, for the present study an effective source height of 300 m AGL was used. The average release rate of oPDCH for the period is about 0.042 g/s. Details on the experiment and measurements can be found in Green (1999) and Isakov (1998). The measurements used for model comparison in the present study are obtained from Isakov (1998), but converted from femtoliters per liter (fl/L) to microgram per unit volume ($\mu g/m^3$).

Dynamic flow and turbulence fields over the study area were simulated with the MIUU model for the period 5/8/92 – 14/8/92. The results are discussed and compared with measurements in Section 3.1. For the present study, only the results of the first three days were used. For use in the dispersion model, the MIUU results, which are stored at 1-hour intervals, were first interpolated to five-minute intervals. Thereafter, the results were interpolated to the dispersion model grid points. Figure 13 (a) and (b) show the interpolated horizontal wind vectors at 100 m AGL at 1200 MST (Mountain Standard Time) on 5/8/92 and 1700 MST on 6/8/92. Note that the wind vectors are plotted only at

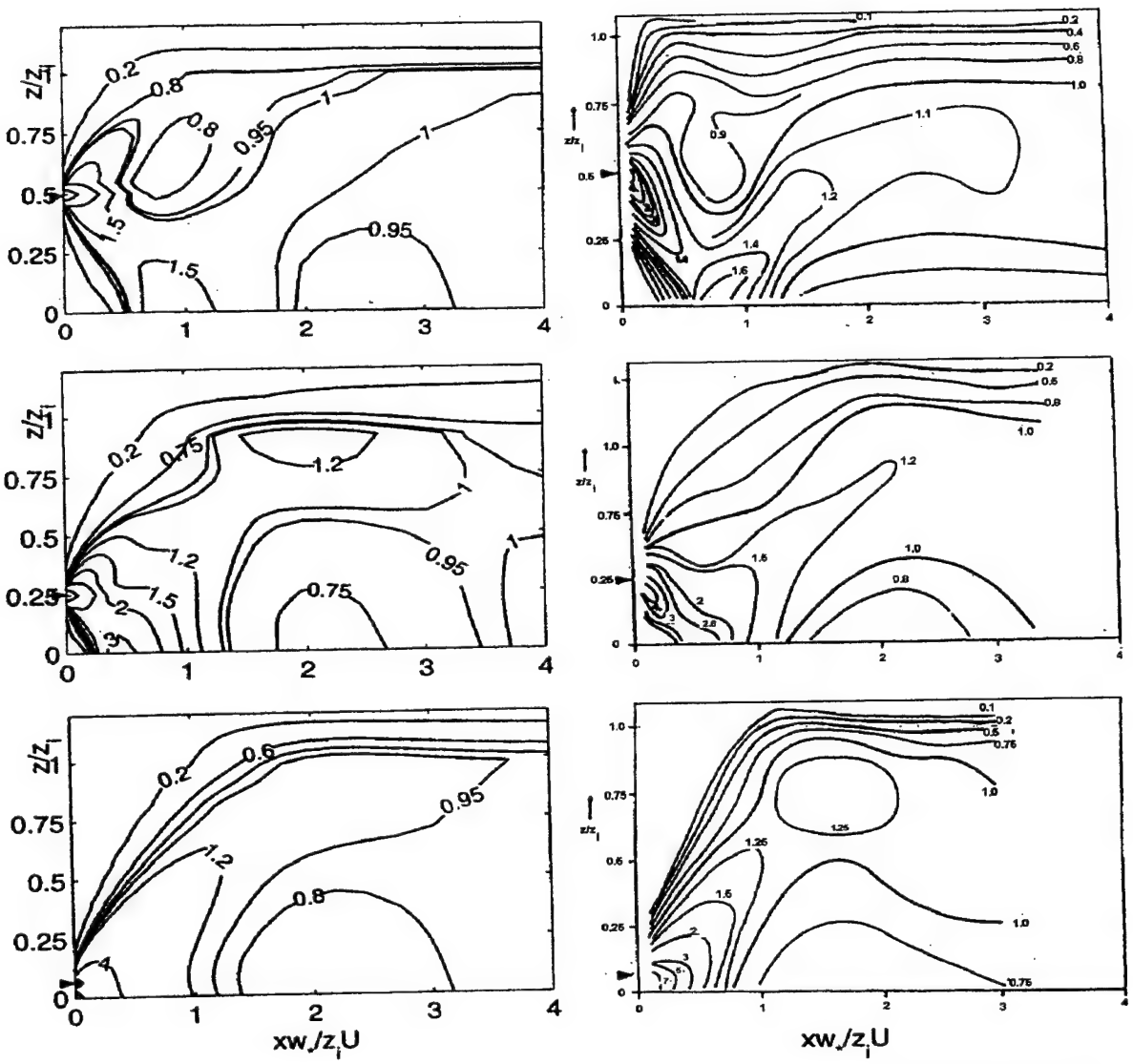

Figure 12. *Contours (in x-z plane) of the dimensionless crosswind integrated concentration simulated by the HOCD model (left) and those from Deardorff and Willis (right) for source heights of 0.062 z_i, 0.25 z_i and 0.5 z_i. Sources are indicated by arrows on the ordinate.*

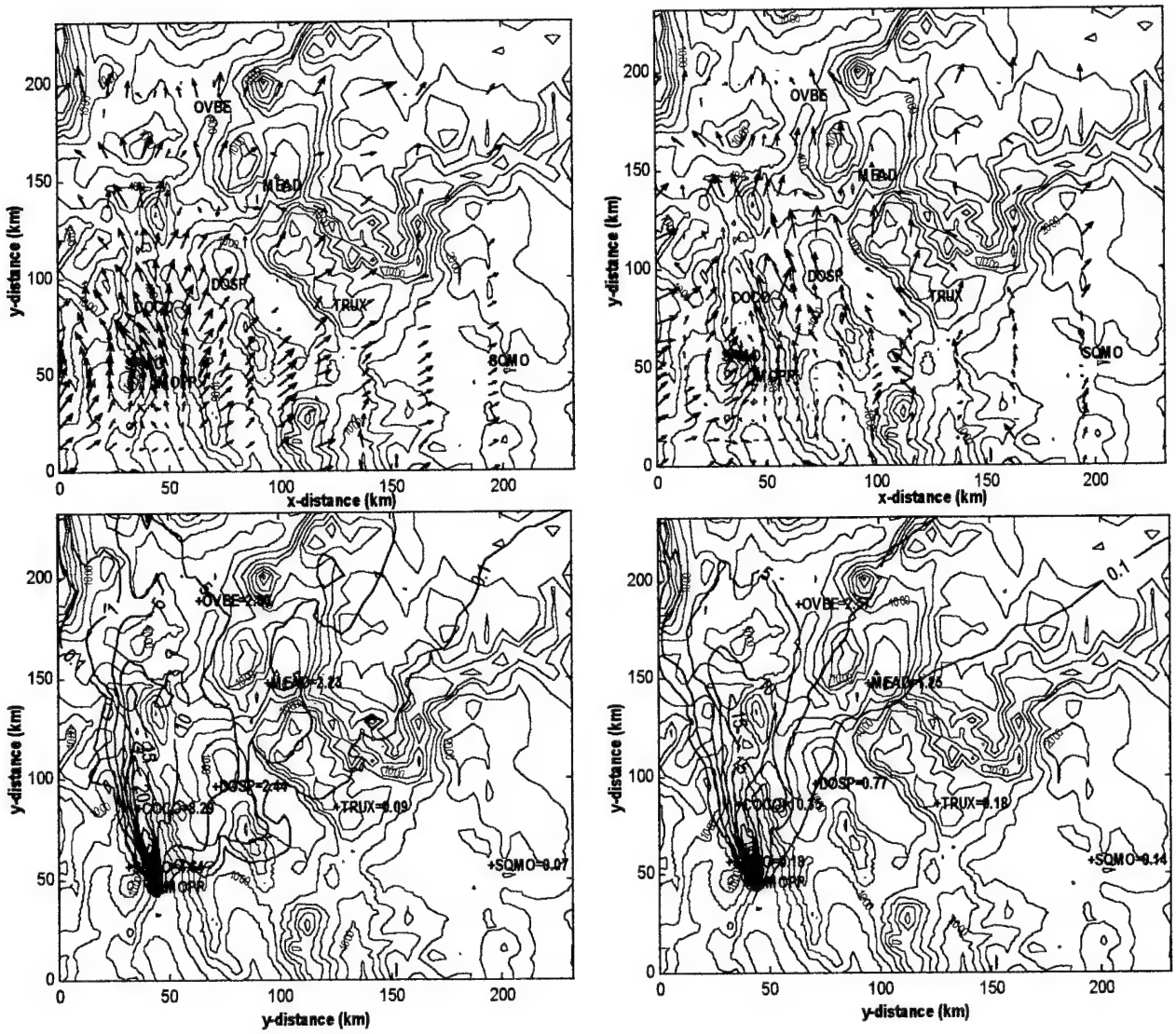

Figure 13. *Model simulations in complex terrain (Colorado River valley) during the MOHAVE field program in summer 1992. Panel (a) and (b) show horizontal wind vectors at 100 m AGL interpolated from the MIUU model results at 1200 MST on 5/8/92 and 0700 MST on 6/8/92, respectively. Maximum vector length is 13 m/s and 19 m/s, respectively. Panel (c) and (d) show the HOCD daily mean of the simulated surface concentration at 0700 MST on 6/8/92 and 7/8/92, respectively. Terrain, receptor locations, and mean concentration measurements are shown in the background. The values of both simulated and measured concentrations are in* 10^{-5} $\mu g/m^3$.

every fifth grid point. Terrain and receptor sites are shown in the background. The results generally show southerly and southwesterly flow in the area. The southerly flow is stronger along the Colorado River valley and follows the bending shape of the valley. Effects of anabatic and katabatic winds along the mountain slopes, due to horizontal pressure gradients created by temperature differences, are visible in the simulated flow at 1200 and 0700 MST, respectively, especially around SPMO and the adjacent mountains.

Tracer release was represented in the dispersion model by a uniformly distributed area source, extending over the nearest four horizontal and three vertical grid points from the source location. The horizontal grid domain used is 81x81 km, with 1 km resolution close to the source. In the vertical, we use 31 grid points, with 50 m resolution close to the release height. Simulated release started at 1200 MST on the first day and continued until 1200 MST on the third day. The daily mean simulated surface concentrations at 0700 MST on the second and third day are presented in Figure 13(c) and (d), respectively. Terrain, receptor sites, and mean measured concentrations at 0700 MST on the two days are shown in the background. The values of both simulated and measured concentrations are in units 10^{-5} $\mu g/m^3$.

From Figure 13 we can see that the simulated concentrations are on the same order of magnitude as the measured ones. The difference between the concentrations could be due to the fact that the release of pollutants in the model did not start at the same time as in the field experiment. Also, insufficient spatial resolution of both the mesoscale and the dispersion model can affect the model results. Nevertheless, the agreement between simulated and measured concentrations is quite good. The model was able to reproduce the spatial pattern of the concentrations over the domain. The model results show that, during stable conditions, the pollutants are transported aloft a few kilometers downwind before reaching the ground surface. During unstable conditions, however, the pollutants reach the ground surface in the vicinity of the release point due to stronger vertical mixing. Moreover, the model simulations show that part of the tracer released from MOPP is transported to the Grand Canyon and its vicinity.

3.2.5 Conclusions

A higher-order closure model suitable for dispersion in complex terrain is developed. The model-simulated features in CBL-dispersion with different source heights have been discussed. The results are in very good agreement with those from tank experiments. Also, the model is applied over a complex terrain near the US Southwest Coast, to study transport and diffusion of tracers released at MOPP during the MOHAVE 1992 field experiment. The simulated pattern and magnitude of concentrations are in good agreement with measurements. The model results also show that part of the pollutants released at MOPP is transported to Grand Canyon and its vicinity. The simulations will be refined in the future with higher grid resolution to obtain better results. Also, the dispersion model simulations will be extended to cover the entire period of the field experiment.

4. Trajectory model

4.1 Model description

This trajectory model uses interpolated three-dimensional wind to calculate the displacement of an air parcel during each time step. Height, given as pressure coordinate, is converted to meters above the sea level by using the hydrostatic equation. Either forward trajectory or backward trajectory can be calculated with this program. For large-scale modeling, for which a rectangular grid is no longer applicable because of a projection problem, the model uses latitudinal and longitudinal to identify grid locations. The model also considers the effect of terrain on the parcel trajectory calculations.

Meteorological data for the research was generated by the Fifth-Generation Penn State/NCAR Mesoscale Model (MM5). Wind components of u, v, and w, pressure, and temperature on all sigma layers at each grid point were used. Terrain information such as latitude, longitude, and height are given at each grid point. Grid interval is set to 3km. Lambert conformal projection was used for domain setting. The projection of the spherical earth onto a plane causes each grid points to have different latitudinal and longitudinal spacing despite a constant distance spacing in km. The trajectory model interpolates from four vertices of a grid cell.

A flow chart of the three-dimensional trajectory program for the meteorological data is given in Figure 14. Considering forward trajectory, the program reads the initial location (x, y, p) of a trajectory. Meteorological data such as wind components, pressure, and temperature are read from two data sets. Grid information such as latitude, longitude, and terrain altitude are also given. The proportional spatial location (xd, yd, pd) of a trajectory with respect to the south west corner of a grid cell is determined from the subroutine LOCATE. The proportional spatial locations have values between 0 and 1. Using the grid wind data of time t, xd, yd, and pd, the wind at the current trajectory location can be calculated. The interpolation is performed at the subroutine INTRPL. In the subroutine DISPL, the displacement of the air parcel is calculated using the relationship: distance (m) = time (s) * velocity (m/s). To calculate backward trajectory, the time step is set to be negative.

It is possible that the calculated new,first guess, trajectory location (x2, y2, p2) is located under the terrain surface. If p2 is larger than the surface pressure at location (x2, y2), the trajectory is considered to be under the surface and two treatment options are then considered. First, the surface-crossing problem is treated by assuming that there is no vertical wind at the surface. Therefore the trajectory, once intercepts the surface, it moves along the terrain surface with only horizontal wind. The other treatment assumes that the air parcel is reflected by the surface at the point where it meets with the surface. Subroutine REFLECT handles the reflection process.

Subroutine LOCATE gives the proportional spatial location (xd, yd, pd) at the new, first guess, trajectory position. With wind (u2, v2, w2) and spatial location (xd, yd, pd), the interpolated wind (up2, vp2, wp2) can be calculated at this trajectory position. The average of (up1, vp1, wp1) and (up2, vp2, wp2) gives the averaged interpolated wind and

Figure 14. *Flow Chart for the 3Dimensional Trajectory Program*

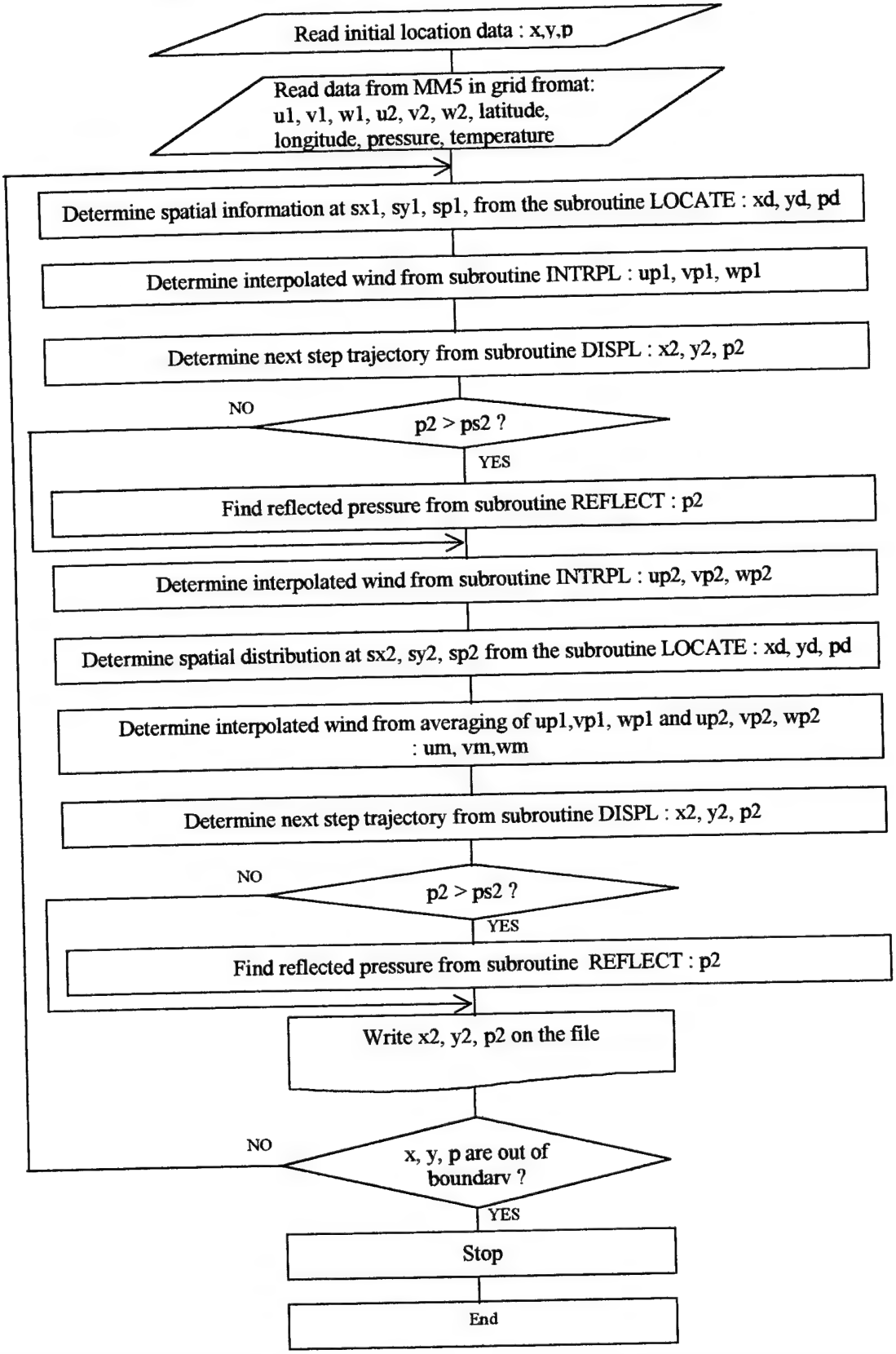

it represents the wind at the given time step of the trajectory (um, vm, wm). Through the subroutine DISPL, the real next step trajectory position (x2, y2, p2) can be calculated using the averaged interpolated wind (um, vm, wm). If p2 is greater that the surface pressure at (x2, y2), reflection will be carried out if the reflection index is on. Otherwise the air parcel keeps following the terrain surface after it meets the surface. This whole process repeats for each time step until the parcel is out of the domain or the time expires.

Figure 15 is an example of a trajectory simulated using the trajectory model. The initial time is 07Z 10 August 1992. The result is for the three-dimensional trajectory with a one-minute time step, using original wind data from the MM5 data and considering reflection when the trajectory meets the surface. The three different trajectories in the top plot reflect the three different initial heights. These initial heights are in the range of the effective plume height from the source during the experiment day. The contours show surface height from sea level. The lower half of Figure 15 shows the vertical displacement along the three trajectories. The dashed lines represent the trajectories and the solid lines represent the surface height along each trajectory. From this figure, not only horizontal variations, but also vertical variations are seen.

4.2. Sensitivity tests

The parameters that affect the trajectory calculations are mostly related to wind direction and speed. Interpolation of the time interval and initial height are important parameters when deciding the pattern of trajectories. Determining whether the considered trajectory is two- or three-dimensional is also an important factor. For instance, choosing different surfaces such as isentropic surface, iso-sigma surface, or three-dimensional trajectory will result in different trajectories. The present study compared the results between trajectories following an iso-sigma surface and trajectories considering vertical wind (3-dimensional). The sensitivity tests are performed by changing one of the following factors: For the wind speed factors, the model was run with three different speed categories, i.e., the original, +10%, and –10% of the modeled speed magnitudes, respectively. For example, with the original vertical wind speed, three trajectories were calculated by only changing the horizontal wind speed among original, +10, and –10% of the modeled speed. The same procedure was repeated with +10% vertical wind speed and –10% vertical wind speed. The sensitivity test includes all factors such as dimension, integration time steps and initial heights. We can then figure out the sensitivity of the trajectory model (Table 2).

Table 3 shows the results of the trajectory ensemble with the same starting time but different parameters. The trajectories starting at 07Z August 1992 are generally toward the northeast but we can see the trajectories have different paths depending on the case. This implies that changing parameters affects the trajectory to limited extent. For other initial times, similar results were obtained.

To estimate the results of a trajectory model, the present study uses tracer potential, which has been developed by Koracin *et. al.* (1999). The tracer potential is given by:

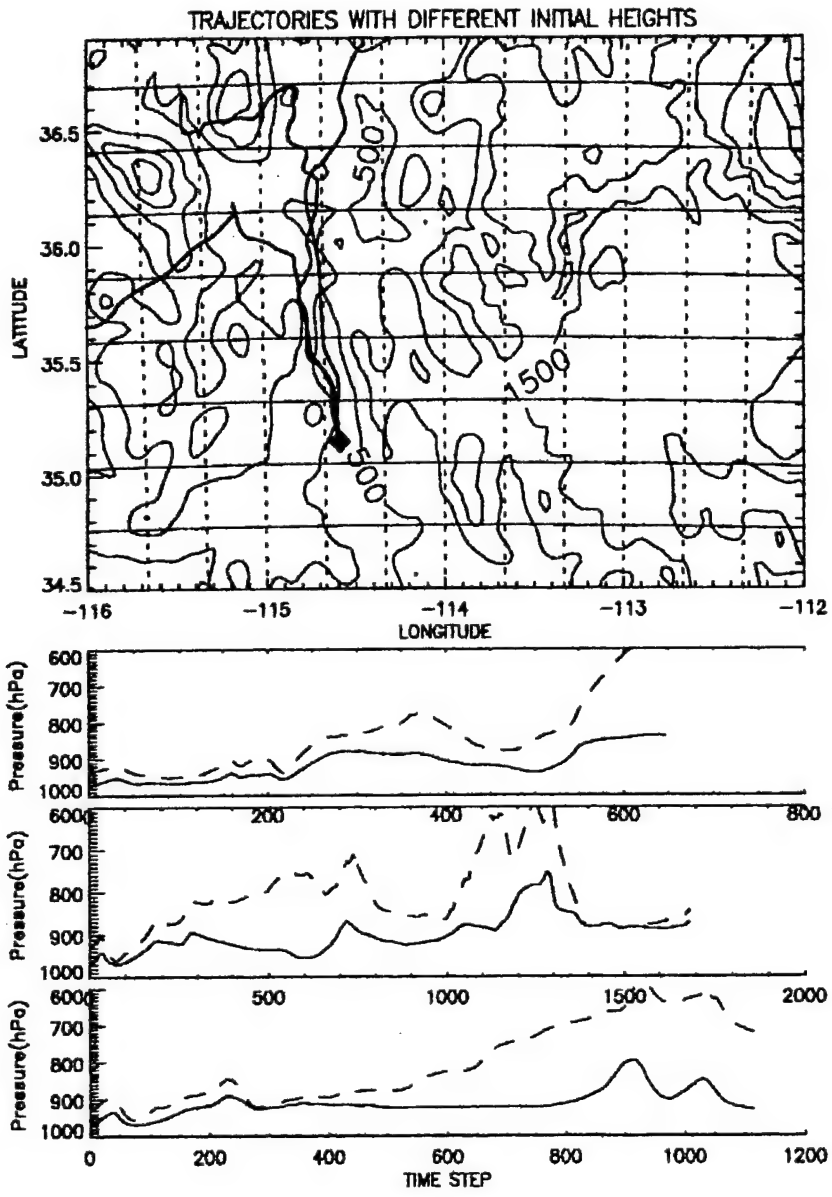

Figure 15. *Trajectories of air parcels released at three different heights (925 mb, 930 mb, 935 mb) at 07Z 10 August 1992 from the source.*

Table 2 *Parameters considered in the sensitivity tests*

Parameters for sensitivity test	**Cases**
Dimension of trajectory	iso-sigma trajectory Three-dimension trajectory
Time step	1 minute 10 minute 30 minute
Initial heights	935mb 930mb 925mb
Horizontal wind	Original wind +10% from original horizontal wind -10% from original horizontal wind
Vertical wind	Original wind +10% from original vertical wind -10% from original vertical wind

Table 3 *Parameter numbers, parameters, and corresponding tracer potential values*

Parameter Number	Parameter*	Tracer Potential
1	f0001D2R0H0V0	0.609
2	f0001D2R0H1V0	0.665
3	f0001D2R0H2V0	0.841
4	f0101D2R0H0V0	0.538
5	f0101D2R0H1V0	0.648
6	f0101D2R0H2V0	0.669
7	f0201D2R0H0V0	0.682
8	f0201D2R0H1V0	0.770
9	f0201D2R0H2V0	0.848
10	f0001D3R0H0V0	1.305
11	f0001D3R0H0V1	1.288
12	f0001D3R0H0V2	1.455
13	f0001D3R0H1V0	1.335
14	f0001D3R0H1V1	1.188
15	f0001D3R0H1V2	1.401
16	f0001D3R0H2V0	1.202
17	f0001D3R0H2V1	1.743
18	f0001D3R0H2V2	1.361
19	f0101D3R0H0V0	0.986
20	f0101D3R0H0V1	1.427
21	f0101D3R0H0V2	1.443
22	f0101D3R0H1V0	1.283
23	f0101D3R0H1V1	1.350
24	f0101D3R0H1V2	1.337
25	f0101D3R0H2V0	1.145
26	f0101D3R0H2V1	1.319
27	f0101D3R0H2V2	1.539
28	f0201D3R0H0V0	1.303
29	f0201D3R0H0V1	1.470
30	f0201D3R0H0V2	1.500
31	f0201D3R0H1V0	1.370
32	f0201D3R0H1V1	1.649
33	f0201D3R0H1V2	1.595
34	f0201D3R0H2V0	1.477
35	f0201D3R0H2V1	1.593
36	f0201D3R0H2V2	1.571

* The parameter 'f' means the considering trajectories are forward trajectories. The following two digits represent initial height as 935mb, 930mb, and 925mb for 00, 01, and 02, respectively. The next two digits representing time step ,in minutes, e.g. '01' means 1min. The number next to the character, 'R' represents either the trajectory considers reflection at the surface ('1') or not ('0'). In the present research, no reflected trajectories are considered and therefore the number is '0'. Digits behind the characters 'H' and 'V' are about wind changes. '0' represents interpolated wind using original data, '1' represents wind speed is 10% more than the original interpolated value, '2' represents wind is 10% less than the original data.

$$TP = \sum_{i=1}^{n} \frac{C_i}{R_i + A}$$

where C_i is the concentration at receptor I, and R_i is the distance between receptor and trajectory. A is a constant, which provides a convergent solution when the trajectory passes over the receptor. The unit for tracer potential is (femtoliter/liter/km).

Koracin *et al.* pointed out that most model evaluation schemes apply a dispersion model to the wind fields and compare dispersion estimates with measured concentration, assuming that measured concentration is real. However, since the wind field simulated by models over complex terrain are usually of poor quality it is important to evaluate the wind fields for dispersion modeling.

In calculating the tracer potential of a trajectory position, concentration at each receptor was weighted by both the magnitude of the receptor's concentration and by the inverse of the distance between the receptor and the trajectory position. This implies that if we compare the weights of two receptors with the same concentration, a receptor closer to an object trajectory has a larger weight than the other receptor. This also implies that if we compare the weights of two receptors with same distance from the object trajectory, the receptor having a larger concentration has a larger weight than the other receptor.

Tracer potential (TP_0) at the source is put as reference value.

$$TP_0 = \sum_{i=1}^{n} \frac{C_i}{R_i + 1}$$

where C_i is concentration at receptor i, and R_i is distance between the source and receptors.

A tracer potential larger than the reference tracer potential implies success of wind field. By comparing tracer potential with the reference tracer potential, we can quantify the success of the wind field itself without relative comparison to other wind fields. Another advantage of the tracer potential method is that even if sampling sights are out of the domain considered for numerical modeling, values from these sampling sites can be used. In other words, there is no waste of observational data from field program.

The results of sensitivity tests by changing parameters are given in Table 3. The results are shown in Figure 16. The sensitivity test shows that three-dimensional trajectories represent better wind fields better than two-dimensional trajectories. For the wind data, using the original MM5 data gives almost the same values at the initial level of 935mb and 925mb. But at the initial level of 930mb, the tracer potential value is 26% lower than other levels, which implies that the contribution of 930mb is less than other levels.

For the three-dimensional cases, the 925mb initial height gives the highest tracer potential value as 1.503([fl/l]*[hr/km]) and the lowest standard deviation value of 0.113. For the two lower levels, the averages and standards deviations of tracer potentials for three-dimensional trajectories don't have significant differences. The average value of tracer potential values including all parameters is 1.394([fl/l)*[hr/km]), and the standard

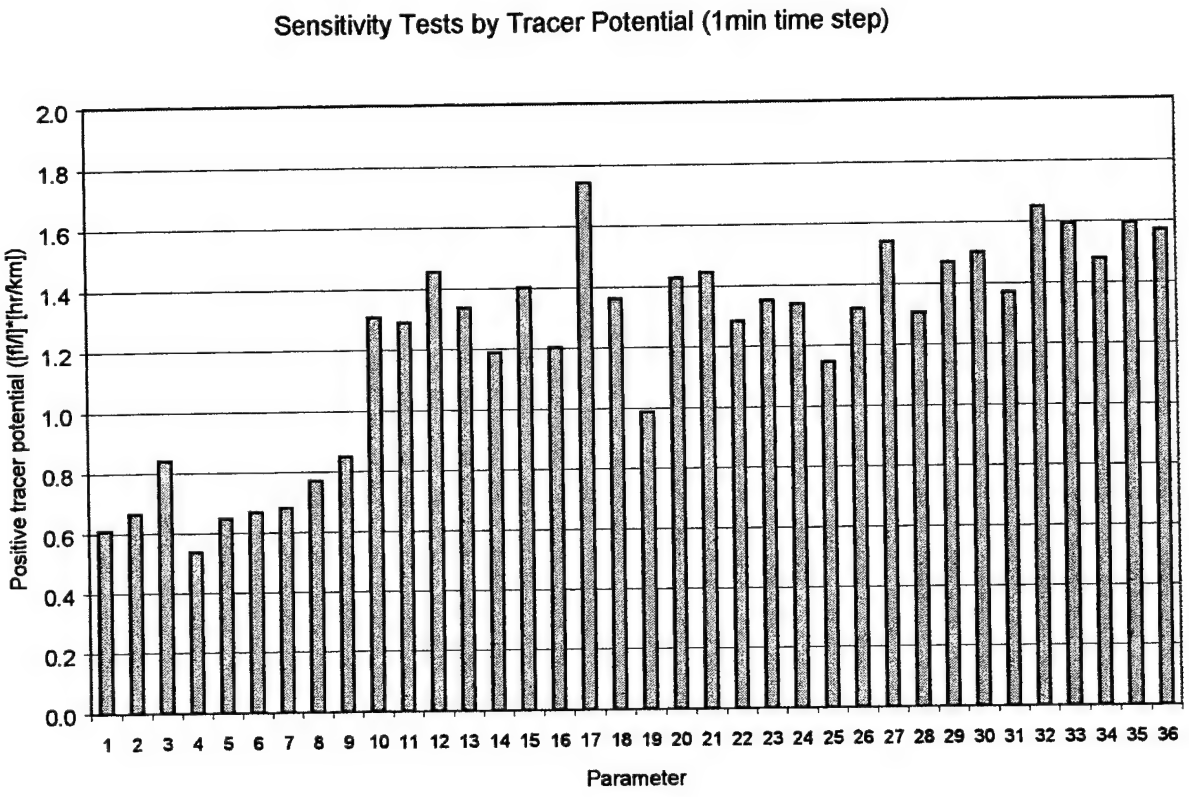

Figure 16. *Sensitivity tests of the trajectory model by using tracer potential*

Table 4. *Average and Standard deviation of tracer potential*

	Average	STD (All)	STD (3D-only)
935mb	1.372	0.334	0.197
930mb	1.355	0.346	0.165
925mb	1.503	0.349	0.113
Total	1.394	0.341	0.116

deviation is 0.166. It seems that the effective plume height of the tracer in 925mb contributes more than at other levels.

4.3 Conclusions

It is shown that a three-dimensional wind field is necessary in trajectory analysis. Reflection at the surface has no major effect on results. At least in this case, the accuracy of wind speed does not contribute greatly to the tracer potential analysis. However, correct wind field data is always beneficial.

This trajectory has many applications. It will be used to determine the aerosol origins in various parts of Texas to see if the chemical content of aerosol has any relationship with rain-cloud formation. We are also planning to use this model to trace the origin of air in the Antarctic during years with El Nino or years with La Nina to see if there are any significant differences between them. This may help in analyzing ancient climate changes.

5. Summary

Three scientific papers and a master's thesis are under preparation from this project. A higher-order closure model suitable for dispersion simulation in complex terrain has been developed. The model-simulated features in CBL-dispersion with different source heights have been performed. The results are in very good agreement with those from the tank experiments. It is shown that the advection terms in the equations for the second order moments that involve concentration are important in simulating the essential features of dispersion. The model shows good agreement when applied to the MOHAVE 1992 field data.

Comparison of wind fields predicted by both the MM5 and the MIUU mesoscale models does not give conclusive statistical answers on which model performs better. It is probably better to use a trajectory model to evaluate the wind field predicted by various models (Koracin et al., 2000).

APPENDIX

A. THE MIUU MODEL

The MIUU model is a three-dimensional, hydrostatic, incompressible, higher order turbulence closure model. The model was developed at the Department of Meteorology, Uppsala University (MIUU) Sweden. A terrain-influenced co-ordinate system, η-system, is used in the model. The basic equations of the model, transformed to this η co-ordinate system are presented below.

$$\frac{dU}{dt}=\left(\frac{s}{s-z_g}\right)^2\frac{\partial}{\partial\eta}K_M\frac{\partial U}{\partial\eta}-\Theta\frac{\partial\Pi}{\partial x}+g\frac{\eta-s}{s}\frac{\partial z_g}{\partial x}-fV_g+fV$$

$$\frac{dV}{dt}=\left(\frac{s}{s-z_g}\right)^2\frac{\partial}{\partial\eta}K_M\frac{\partial V}{\partial\eta}-\Theta\frac{\partial\Pi}{\partial y}+g\frac{\eta-s}{s}\frac{\partial z_g}{\partial y}+fU_g-fU$$

$$\frac{\partial V}{\partial t}+\frac{\partial V}{\partial y}+\frac{\partial W}{\partial z}=\frac{1}{s-z_g}\left(U\frac{\partial z_g}{\partial x}+V\frac{\partial z_g}{\partial y}\right)$$

$$\frac{d\Theta}{dt}=\left(\frac{s}{s-z_g}\right)^2\frac{\partial}{\partial\eta}K_H\frac{\partial\Theta}{\partial\eta}+\sigma_r$$

$$\frac{\mathrm{dR}}{\mathrm{dt}}=\left(\frac{\mathrm{s}}{\mathrm{s}-\mathrm{z_g}}\right)^2\frac{\partial}{\partial\eta}\mathrm{K_R}\frac{\partial\mathrm{R}}{\partial\eta}$$

$$\frac{dq^2}{dt}=\left(\frac{s}{s-z_g}\right)^2\frac{\partial}{\partial\eta}\left(\frac{5}{3}\alpha_1 q\lambda\frac{\partial q^2}{\partial\eta}\right)+2\left(\frac{s}{s-z_g}\right)^2K_M\left[\left(\frac{\partial U}{\partial\eta}\right)^2+\left(\frac{\partial V}{\partial\eta}\right)^2\right]-2\frac{s}{s-z_g}\frac{g}{\Theta_0}K_H\frac{\partial\Theta}{\partial\eta}-2\frac{q^3}{B_1\lambda}$$

$$\frac{\mathrm{d}}{\mathrm{dt}}=\frac{\partial}{\partial\mathrm{t}}+\mathrm{U}\frac{\partial}{\partial\mathrm{x}}+\mathrm{V}\frac{\partial}{\partial\mathrm{y}}+\mathrm{W}\frac{\partial}{\partial\eta}$$

where W is the mean vertical wind speed in the terrain following coordinate system, η. For more information see e.g. Enger (1986), Tjernström, (1988), Andrén (1990)

B. LENGTH SCALE FORMULATION

The turbulent length scales used in the model scales are parameterized in a similar fashion with Enger (1986, 1990) and included the modification by Andrén (1990). It is supposed that all the length scales are to be proportional to each other. This means one only needs to determine one length scale (λ), which is sufficiently general to handle various types of flow in the atmosphere.

Unstable surface layer:

$$\lambda = \frac{\kappa z}{B_1}\left[\frac{\left(1-3\frac{z}{L}\right)^{2/3}+2\left(6.2-0.52\frac{z_i}{L}\right)^{2/3}}{1+0.5\left|\frac{z}{L}\right|^{2/3}}\right]^{3/2} \qquad \text{(B1)}$$

Unstable mixed layer:

$$\lambda = \frac{\left[0.7+1.75\left(\frac{z}{z_i}\right)^{2/3}-1.65\left(\frac{z}{z_i}\right)^{4/3}\right]^{3/2} z_i}{B_1\left[0.55\left(\frac{z}{z_i}\right)^{-1/3}-0.3\right]} \qquad \text{(B2)}$$

A smooth transition is obtained between (B1) and (B2) by taking the minimum of the two expressions.

Neutral and stable boundary layer:

$$\frac{1}{\lambda} = \frac{\min\left\{1+3.3\frac{z}{L},4.3\right\}}{\kappa z} + \frac{1}{0.1\frac{\int_0^\infty qzdz}{\int_0^\infty qzdz}} \qquad \text{(B3)}$$

At the top of the boundary layer these formulation are limited by using the minimum of the stability-dependent formulation.

$$\lambda = C_B\frac{q}{\omega_B} \quad , \qquad \text{(B4)}$$

where ω_B is the Brunt-Väisälä frequency and the neutral form of equation (B3). For the constant C_B a value of 0.5 is used. For constant B_1 a value of 21.33 is used, which incorporate the parameterization of 'wall effect' at surface as introduced by Andrén (1990). For more information on the calculations of the constants see Enger (1986, 1990a) and Andrén (1990).

REFERENCES:

Andrén A. (1987) A combined first-order closure/Gaussian dispersion model. Atmospheric Environment **21,** 1045-1058.

Andrén A. (1990) Evaluation of a turbulence closure scheme suitable for air-pollution applications. J. Appl. Meteorol., **29,** 224-239.

Belward, A.S. (1996), 'The IGBP-DIS global 1 km land cover data set (DISCover)-proposal and implementation plans', *IGBP-DIS Working Paper*, No. 13, Toulouse, France, 61 pp.

Davies, H.C. (1976), 'A lateral boundary formulation for multi-level prediction models', *Quart. J. R. Met. Soc.*, Vol. 102, pp. 405-418.

Deardorff J. W. and Willis G. E. (1975) A parameterization of diffusion into the mixed layer. J. appl. Met. **14,** 1451-1458.

Donaldson C. du P. (1973) Construction of a dynamic model of the production of atmosphere turbulence and the dispersal of atmospheric pollutants. In Workshop on micrometeorology (edited by Haugen D.A.)Amer. Meteorol. Soc. Pub.

Egan B. A. (1984) Transport and diffusion in complex terrain (review). Boundary-Layer Met. **30,** 3-28.

Enger L. (1986) A higher order closure model applied to dispersion in a convective PBL. Atmospheric Environment **20,** 879-894.

Enger L. (1990a) Simulation of dispersion in moderately complex terrain-Part A. The fluid dynamic model. Atmospheric Environment **24,** 2431-2446

Enger L. (1990b) Simulation of dispersion in moderately complex terrain-Part B. The higher order closure dispersion model. Atmospheric Environment **24,** 2447-2455

Enger L. (1990c) Simulation of dispersion in moderately complex terrain-Part C. A dispersion model for operational use. Atmospheric Environment **24,** 2457-2471

Enger L. and Grisogono B. (1997) The response of bora-type flow to sea surface temperature. Q. J. R. Meteorol. Soc. **124,** 1227-1244

Enger L. and Koracin D. (1995) Simulation of dispersion in complex terrain using a higher-order closure model. Atmospheric Environment **29,** 2449-2465

Enger, L., D. Koracin, and X. Yang (1993), 'A numerical study of boundary layer dynamics in a mountain valley. Part 1. Model validation and sensitivity experiments', *Bound.-Layer Meteor.*, Vol. 66, pp. 357-394.

Fackrell J. E. and Robins A.G. (1982) Concentration fluctuations and fluxes in plumes from point source in a turbulent boundary layer. J. Fluid Mech. **117,** 1-26

Green, M.C. (1999), 'The Project MOHAVE tracer study: Study design, data quality and and overview of results', *Atmos. Environ.*, Vol. 33, pp. 1955-1968.

Grell, G.A., J. Dudhia, and D.R. Stauffer (1995), 'A description of the Fifth-Generation Penn State/ NCAR Mesoscale Model (MM5)', *NCAR Tech. Note TN-398*, 122 pp. [Available from NCAR, P.O. Box 3000, Boulder, CO. 80307].

Hunt J.C.R., Puttok J.S. and Snyder W.H. (1979) Turbulent diffusion from a point source in stratified and neutral flows around a three-dimensional hill-I. Diffusion equation analysis. Atmospheric Environment **13,** 1227-1239.

Isakov, V. (1998), 'Evaluation of Atmospheric and Dispersion Models in Complex Terrain by Using Tracer Measurements', *Ph.D. Thesis*, 119 pp. [Available from Division of Atmospheric Sciences, Desert Research Institute, 2215 Raggio Parkway , Reno, NV 89512]

Kalnay E., M. Kanamitsu, R. Kistler, W. Collins, D. Deaven, L. Gandin, M. Iredell, S. Saha, G. White, J. Woollen, Y. Zhu, M. Chelliah, W. Ebisuzaki , W. Higgins, J. Janowiak, K.C. Mo, C. Ropelewski, J. Wang, A. Leetmaa, R. Reynolds, R. Jenne, D. Joseph (1996), 'The NCEP / NCAR 40-year reanalysis project', *Bull. Amer. Meteor. Soc.*, Vol. 77, No. 3, pp. 437-471.

Koracin, D., J. Frye, and V. Isakov (2000), 'A Method of Evaluating Atmospheric Models Using Tracer Measurements', *J. Appl.Meteor.*, Vol. 39, No. 2, pp. 201-221.

Lamb R.G. (1978) A numerical simulation of dispersion from an elevated point source in the convective planetary boundary layer. Atmospheric Environment **12,** 1297-1304.

Lamb R.G. (1979) The effects of release height on material dispersion in the convective planetary layer. Preprint vol. Amer. Meteor. Soc. Fourth Symposium on Turbulence, diffusion and Air Pollution, Reno, N.V.

Lamb R.G. (1982) Diffusion in the convective boundary layer. In Atmospheric Turbulence and Air Pollution Modelling (edited by Nieuwstadt F.T.M. and van Dop H.) pp. 159-229. D. Reidel, Dodrecht.

Lumely J.L. (1975) Prediction methods for turbulent flows VKI-LS 76, Rhode-St-Genese, Belgium.

Mellor G.L. (1973) Analytical prediction of the properties of stratified planetary surface layers. J. atmos. Sci. **30,** 1061-1069.

Mellor, G.L. and T.Yamada (1974), 'A hierarchy of turbulence closure models for planetary boundary layers', *J. Atmos. Sci.*, Vol. 31, pp. 1791-1806.

Mistra P.K. (1980) Dispersion from tall stacks into a shore environment. Atmospheric Environment **14,** 1213-1215.

Moninger, W. R., Eberhard, W.L., Briggs G. A., Kropfli R.A. and Kaimal, J.C. (1983) simultaneous Radar and Lidar Observations of plume from continuous point sources. 21st Radar Meteorological conference, Amer. Meteorol. Soc., Boston, MA, 246-250.

Nieuwstadt F.T.M. (1980) Application of mixed-layer similarity to the observed dispersion from a ground level source. J. appl. Met. **19,** 157-162.

Pielke, R.A. (1984), *Mesoscale Meteorological Modeling*, Academic Press, Orlando, San Diego, San Francisco, New York, London, Toronto, Montreal, Sydney, Tokyo.

Pitchford, M., M. Green, H. Kuhns, I. Tombach, W. Malm, M. Scruggs, R. Farber and V. Mirabella (1999), *Project Mohave, Peer Review Version, Draft Final Report*, National Oceanic and Atmospheric Administration (NOAA), Las Vegas (NV).

Segal M., McNider R.T., Pielke R.A. and McDougal D.S. (1982) A numerical model simulation of the regional air pollution meteorology of the Greater Chesapeake Bay area- summer day case study. Atmospheric Environment **16,** 1381-1397.

Shir C.C. (1973) A preliminary numerical study of atmospheric turbulent flows in the idealized planetary boundary layer. J. atmos. Sci. **30,** 1327 1339.

Tjernström, M (1988) Numerical simulations of boundary layer cloud on the meso-scale. Part I: The influence of terrain height differences. Boundary-Layer Meteorol., **44,** 33-72.

Uliasz M. (1994) Lagrangian particle dispersion modelling in mesoscale applications. In Environmental modelling II (edited by Zannetti, P.), Computational Mechanics Publications, 71 - 102.

Willis G.E. and Deardorff J.W. (1978) A laboratory study of dispersion from an elevated source within a modeled convective planetary boundary layer. Atmospheric Environment **12,** 1305-1311.

Willis G.E. and Deardorff J.W. (1981) A laboratory study of dispersion from a source in the middle of the convective mixed layer. Atmospheric Environment **15,** 109-11 7.

Yamada, T. (1985), 'Numerical Simulations of Valley Ventilation and Pollutant Transport. Proc.7th Symposium on Turbulence and Diffusion with Boulder, Colorado. Amer. Meteor. Soc. 312-314.

NOMENCLATURE

Symbols that are defined in the text are not included in this list

C	mean concentration
c'	fluctuating part of concentration
D	molecular destruction term
f	Coriolis parameter
g_i	acceleration of gravity, $g_i = (0,0,-g)$
K	general notation for scalar eddy transfer coefficient, e.g. K_H, and K_M are eddy transfer coefficients for heat and momentum, respectively
L	Monin-Obukhov's length
P_{rt}	Prandtl number, $P_{rt} \equiv -\overline{u'w'}\frac{\partial \Theta}{\partial z}\Big/\left(-\overline{w'\theta'}\frac{\partial U}{\partial z}\right)$
p'	fluctuating part of the pressure
q^2	mean double turbulent energy
Q	source strength
R	mean specific humidity
S_c	Sinks and sources
s	Model top
U,V,W	mean wind speed in x, y, and η- direction, respectively
U_g,V_g	geostrophic wind in x- and y-direction, respectively
U_i	mean wind in tensor form
u',v',w'	fluctuation part of the wind speed in x, y, and z- direction, respectively
u'_i	fluctuation part of the wind speed in tensor form

u_* friction velocity

w_* convective velocity scale, $w_* = (z_i \overline{w'\theta_0'} g / \Theta)^{1/3}$

x,y,z coordinate in west-east, south-north, and vertical direction, respectively

x_i coordinate in tensor form

z_g terrain height

z_i convective boundary layer height defined as the height of the minimum heat flux

$\alpha_1, \alpha_2, \beta_1, \beta_H$ constants

λ characteristic turbulent length scale

η terrain influenced coordinate system ($= s\frac{z - z_g}{s - z_g}$)

ρ density

σ_r radiative heating/cooling rate

Θ mean potential temperature

θ' fluctuating part of the potential temperature

Π a scaled pressure, the so-called Exner function